

# Multi-Area Throughput and Energy Optimization of UAV-aided Cellular Networks Powered by Solar Panels and Grid

Luca Chiaraviglio,<sup>(1,2)</sup> Fabio D'Andreagiovanni,<sup>(3,4)</sup> William Liu,<sup>5</sup> Jairo A. Gutierrez,<sup>5</sup>

Nicola Blefari-Melazzi,<sup>(1,2)</sup> Kim-Kwang Raymond Choo,<sup>6</sup> Mohamed-Slim Alouini<sup>7</sup>

1) University of Rome Tor Vergata, Italy, {luca.chiaraviglio,blefari}@uniroma2.it

2) Consorzio Nazionale Interuniversitario per le Telecomunicazioni, Italy

3) National Center for Scientific Research (CNRS), France, d.andreagiovanni@hds.utc.fr

4) Heudiasyc UMR 7253, Sorbonne Universités, Université de Technologie de Compiègne, CNRS, France

5) Auckland University of Technology, New Zealand, {jairo.gutierrez, william.liu}@aut.ac.nz

6) The University of Texas at San Antonio, Texas, raymond.choo@fulbrightmail.org

7) Computer, Electrical, and Mathematical Science and Engineering (CEMSE) Division, King Abdullah University of Science and Technology (KAUST), Thuwal, Makkah Province, Saudi Arabia, slim.alouini@kaust.edu.sa

**Abstract**—Small Cells (SCs) mounted on top of Unmanned Aerial Vehicles (UAVs) can be used to boost the radio capacity in hotspot zones. However, UAV-SCs are subject to tight battery constraints, resulting in frequent recharges operated at the ground sites. To meet the UAV-SCs energy demanded to the ground sites, the operator leverages a set of Solar Panels (SPs) and grid connection. In this work, we demonstrate that both i) the level of throughput provided to a set of areas and ii) the amount of energy that is exchanged with the grid by the ground sites play a critical role in such UAV-aided cellular network. We then formulate the J-MATE model to jointly optimize the energy and throughput through revenue and cost components. In addition, we design the BBSR algorithm, which is able to retrieve a solution even for large problem instances. We evaluate J-MATE and BBSR over a realistic scenario composed of dozens of areas and multiple ground sites, showing that: i) both J-MATE and BBSR outperform previous approaches targeting either the throughput maximization or the energy minimization, and ii) the computation time and the memory occupation of BBSR are reduced up to five orders of magnitude compared to J-MATE.

**Index Terms**—cellular networks, throughput and energy management, UAV, renewable energy

## 1 INTRODUCTION

The potential to utilize Unmanned Aerial Vehicles (UAVs) to carry Small Cell (SC) capabilities is a topic of ongoing interest in the research and practitioner community, as evidenced by the seminal works of [1], [2], [3] and the recent surveys/tutorials [4], [5]. In comparison to a traditional cellular network composed of fixed Macro Cells (MCs), UAV-SCs provide: i) coverage flexibility [6], as it is possible to selectively choose the areas to be served by UAV-SCs over time and space, ii) performance increase [7], due to the Line Of Sight (LOS) and proximity conditions experienced on the radio link between the users and the serving UAV-SCs, and iii) CAPital EXPenditures (CAPEX) reduction [8], as the number of sites to host fixed MC capabilities is decreased. In this context, a viable option is to deploy a UAV-aided cellular network [9], in which a small number of MCs provide basic performance to users over the territory, while UAV-SCs are instead used to improve the capacity in selected areas.

Although the utilization of a UAV-aided cellular network is a promising approach for the deployment of future cellular networks [10], there are a number of technological challenges that need to be taken into account in real-world implementations of such architecture [5]. One key issue is the energy consumption of UAV-SCs [4]. Compared to a fixed MC, which is connected to the electricity grid, the battery capability of a UAV-SC is generally limited [11].

Consequently, the coverage of an area served by a UAV-SC has to be scheduled inside a mission [12] to always ensure an adequate battery level and avoid its discharge before the mission completion. In this context, each UAV-SC mission starts and ends at a set of ground sites, which provide recharging capabilities to the UAV-SCs. Since the cumulative energy required by the UAV-SCs that need to be recharged in a ground site may be significant [8], each ground site generally needs to consider (or attempts to leverage): i) the energy locally produced by a set Solar Panels (SPs) and ii) the connection to the electricity grid. In this way, the ground site can satisfy the UAV-SCs demand by buying energy from the grid when the energy produced by SPs is not sufficient and/or available.

In such a scenario, it is clear that the energy-efficient management of UAV-SCs missions is a crucial aspect faced by the operator. From an OPerating EXPenses (OPEX) perspective, the operator should minimize the use of UAV-SCs, in order to: i) limit the number of UAV-SC recharges, and ii) maximize the amount of SP energy that is sold to the grid. However, this policy contradicts the need to provision the radio capacity to users, which targets the maximization of the UAV-SCs deployment to maximize the performance of the covered areas. In addition, the amount of throughput provided to the users may be linked to the revenue gained by the operator from users' subscription plans. This is

especially true for data-hungry services like adaptive video streaming, Internet of Things (IoT) subscriptions, social media, which may be on a pay-as-you-go fee plan.

The optimization of the different costs/revenues terms derived from the management of the UAV-SCs is therefore a challenging aspect for an operator. In this context, a natural question arises: is it possible to jointly optimize the energy bought from the grid, the energy sold to the grid and the throughput provided by a UAV-aided cellular network architecture to maximize the global operator's revenue? The goal of our work is to answer this question, which, to the best of our knowledge, has received very little attention by the research community so far. Specifically, we develop a framework that allows the operator to control: i) the throughput provided over the territory by a set of MCs and a set of UAV-SCs, ii) the UAV-SCs missions over time and space, iii) the UAV-SC energy constraints and iv) the energy balance between the SPs production, the energy bought from the grid and the energy sold to the grid in the ground sites.

Our contributions are summarized as follows:

- we model the Radio Resource Management (RRM) operated by the MCs and the UAV-SCs, through the BandWidth (BW) that each MC distributes over the territory. This contribution is inline with other works in the literature (e.g., [9]), which adopt joint RRM between MCs and UAV-SCs. However, unlike prior approaches that do not consider a joint RRM and energy strategy, we seek to address both in our work. Specifically, we model the MC bandwidth redistribution, which is expressed through the amount of BW that is released to a MC when an area starts to be covered by a UAV-SC;
- we model the UAV-SCs missions and energy levels over time and 3D-space domains through a graph-based approach. In other words, unlike the approach presented in [13], we target a novel problem where multiple areas and multiple sites are considered;
- we introduce constraints to model the energy balance at the ground sites;
- we formalize an innovative optimization model, JOINT MANAGEMENT OF MULTI-AREA THROUGHPUT AND ENERGY (J-MATE), to balance throughput/revenue and energy costs;
- we design a new algorithm, BALANCE ENERGY BOUGHT, ENERGY SOLD AND THROUGHPUT REVENUE (BBSR), which targets the solution of the problem in large instances, comprising dozens of areas and multiple ground sites;
- we consider a scenario, located in Rotorua (New Zealand), which integrates real-world measurements and parameters. Therefore, we also validate through a real testbed the UAV-SC energy consumption model defined in this work;
- we perform an in-depth analysis of the performance of J-MATE and BBSR compared to a set of other strategies used as reference;
- we consider a wide set of metrics to more accurately benchmark our proposed approach with the reference strategies.

The goal of this paper is to: i) model a complex system containing various independent parameters and ii) provide a unique solution striking a balance between revenues and costs.

Our results demonstrate that J-MATE and BBSR are very effective in managing the revenues and costs components of the UAV-aided cellular architecture. Specifically, by leveraging a weight parameter assigned to the throughput, the operator can achieve: i) the maximization of the energy sold to the grid, ii) the maximization of the throughput provided to a set of areas, or iii) a balanced strategy between i) and ii). In addition, we also show that BBSR reduces both the computation time and the memory occupation up to five orders of magnitude compared to J-MATE. We believe that our outcomes may trigger future research in the field, which includes: i) the cooperation of multiple UAV-SCs to cover the same area and realize beyond 5G services; and ii) the design of machine learning-based algorithms to provide the capability to react in real time to unexpected events (e.g., bad weather conditions, UAV-SCs failures, user mobility).

The rest of the paper is organized as follows. Sec. 2 briefly reviews the related literature. Sec. 3 highlights the main features of the UAV-aided cellular architecture considered in this work. Sec. 4 and Sec. 5 present J-MATE and BBSR, respectively. The real-world scenario is shown in Sec. 6. Performance evaluation of the considered strategies is presented in Sec. 7. Finally, Sec. 8 concludes our work.

## 2 RELATED WORK

Tab. 1 summarizes the positioning of this work compared to the literature, considering: i) the trajectory control of UAV-SCs (considered or not by the related work), ii) the computation of the trajectory (through a 2D plane, a 3D plane, or a multi-period (MP) graph), iii) the granularity of the targeted optimization (in terms of single user or whole areas), iv) the RRM policy implemented (none, frame-based, unit-based, subcarrier-based or BW-based), v) the number of fixed MCs assumed in the scenario (none, one single MC, or multiple MCs), vi) the considered number of UAV-SCs (single or multiple), vii) the presence of constraints to control the UAV-SCs energy consumption, viii) the presence of constraints to control the site energy production/consumption, and ix) the pursued approach (model-based, optimization-based, and/or algorithm-based).

Several considerations can be derived by observing in more detail Tab. 1. First of all, the literature on the topic may appear pretty vast at a first glance. However, many works introduce different simplifications, like the computation of the UAV-SCs trajectory in the 2D plane (i.e., not considering the 3D space), no RRM, no fixed MCs, one single UAV-SC, and no energy constraints for the UAV-SCs and/or the ground sites. Although we recognize the importance of such previous works, we point out that our goal is to consider a realistic UAV-aided cellular architecture, where: i) we control the UAV-SCs trajectories in the 3D space through an MP graph, ii) we consider the BW provided to each area as the main resource to be managed through the RRM, iii) we focus on a scenario where each area may be served by multiple fixed MCs or by one UAV-SC - we also provide evidence from real measurements that the condition in which

TABLE 1  
Positioning of this work w.r.t. the literature.

Work	Trajectory Control	Trajectory Computation	Target	RRM	Fixed MCs	Number of UAVs	UAV Energy Constraints	Site Energy Constraints	Approach
Mozaffari <i>et al.</i> [14]	-	-	Areas	-	Multiple	Multiple	-	-	Opt.
Sharma <i>et al.</i> [7]	-	-	Areas	-	Multiple	Multiple	-	-	Alg.
Qureshi <i>et al.</i> [15]	-	-	Areas	-	Multiple	Multiple	-	-	Model
Mignardi <i>et al.</i> [16]	Yes	2D-plane	Areas	-	Multiple	Multiple	-	-	Alg.
Jeong <i>et al.</i> [17]	Yes	2D-plane	Users	Yes (frames)	Multiple	Single	Yes	-	Opt.,Alg.
Verdone <i>et al.</i> [18]	Yes	2D-plane	Areas	Yes (units)	Multiple	Single	-	-	Alg.
Wu <i>et al.</i> [19]	Yes	2D-plane	Users	-	-	Multiple	-	-	Opt.,Alg.
Zhu <i>et al.</i> [20]	Yes	2D-plane	Areas	-	-	Single	Yes	-	Opt.,Alg.
Li <i>et al.</i> [21]	Yes	3D-plane	Users	Yes (subcar.)	-	Single	-	-	Opt.,Alg.
Mardani <i>et al.</i> [22]	Yes	2D-plane	Areas	-	-	Single	Yes	-	Alg.
Zeng <i>et al.</i> [23]	-	-	Users	-	Multiple	Multiple	-	-	Model
Trotta <i>et al.</i> [24]	-	-	Areas	-	-	Multiple	Yes	Yes (Rec. actions)	Opt.,Alg.
Wu <i>et al.</i> [25]	Yes	2D-plane	Users	-	-	Multiple	Yes	-	Model
Hua <i>et al.</i> [26]	Yes	2D-plane	Users	Yes (BW)	Single	Single	Yes	-	Opt.,Alg.
Sun <i>et al.</i> [27]	Yes	3D-plane	Users	Yes (subcar.)	-	Single	Yes	-	Opt.,Alg.
Chiaraviglio <i>et al.</i> [13]	Yes	MP graph	Areas	Yes (BW)	Single	Multiple	Yes	Yes (Single Site)	Opt.
This work	Yes	MP graph	Areas	Yes (BW)	Multiple	Multiple	Yes	Yes (Multiple Sites)	Opt.,Alg.

multiple MCs serve the same area is common in currently deployed cellular networks (especially in zones located at the cell border), iv) we jointly control a set of multiple UAV-SCs and their actions over time (e.g., covering, moving, recharging), v) we explicitly model the energy constraints of the UAVs and of the ground sites, vi) we tackle the problem by providing the J-MATE formulation and the BBSR algorithm.

Actually, the closest paper to this work is [13], where the authors have targeted the optimization of the area throughput and the grid-connected microgeneration in a UAV-based scenario. However, as outlined in Tab. 1, our work is radically different from [13] under the following aspects: i) we consider an architecture composed of multiple fixed MCs (and not a single one like in [13]) to better reflect the deployment of a realistic cellular network, ii) we assume multiple sites providing energy capabilities to the UAVs (and not a single site like in [13]) - in this way, each UAV is able to choose at which site to recharge, iii) we face the problem not only from the optimization perspective, but also by designing the BBSR algorithm, which is able to efficiently retrieve a solution in a limited amount of time and with limited memory resources. In addition, another key feature of this work (and not covered at all by previous ones) is the validation of the UAV-SC energy model (derived from [27]) through the measurements performed on a real UAV-based testbed.

Summarizing, we face a scenario where the UAV-SCs offer coverage capabilities to a set of areas. Each area may be served by a set of multiple fixed MCs or by a UAV-SC. We model the UAV-SC trajectories (and their actions) as an MP graph, in order to precisely control the UAV-SCs positions and actions in the 3D space. We consider a set of ground sites offering recharging capabilities to the UAV-SCs. We take into account the energy management of the UAV-SCs, by properly considering the impact of the different UAV-SC actions on the battery level. In addition, we consider the ground site energy constraints in terms of: i) energy produced by SPs, ii) energy bought from the grid, iii) energy sold to the grid. Compared to previous work, we propose a new approach for a UAV-aided cellular network, which allows the operator to jointly control: i) the management of the radio resources (in terms of BW) to provide the

throughput over a set of areas, ii) the amount of energy exchanged with the grid by each ground site, iii) the actions, the trajectories and the battery levels of a set of UAV-SCs.

### 3 ARCHITECTURE

We describe our architecture through a set of main building blocks, reported in the following subsections.

#### 3.1 Definition of Radio Resources

In our framework, the radio resources are expressed in terms of BandWidth (BW) assigned to a set of areas, where users and/or their activity tend to concentrate. Clearly, in a real-world network, the radio resources (e.g., Resource Blocks in LTE) have to be split among users in the area. Moreover, some radio resources have to be allocated to the control channels. However, the evaluation of the actual level of performance achieved by single users is not the main goal of this work, as this feature requires to consider user channel conditions and the discrete amount of radio resources delivered to each user. Consequently, this step may increase the problem complexity to a large extent. Eventually, the computation of the radio resources that are allocated to the single users can be performed after the BW allocation to the area, e.g., by efficiently scheduling the radio resources to each user in the area.

#### 3.2 UAV-SCs to improve the area throughput

The second building block of our architecture is designed to improve the throughput for each area. Each UAV carries a Small Cell (SC), whose frequency band is separated from the one used by the fixed Macro Cells (MCs). Therefore, there is no interference between a UAV-SC and a fixed MC.<sup>1</sup> Focusing on the interference between UAV-SCs, we assume that each area is served by at most one UAV-SC. In addition, the positions of the areas and their coverage size, which are provided as input to our problem, are designed

1. In this paper, we assume that the radio link between the UAV-SC and the ground site, which provides connectivity to the rest of the Internet, does not use the same portion of BW of the MCs or the UAV-SCs. This link may be realized considering other radio technologies, such micro-wave links or Free Space Optical (FSO) links. We leave the investigation of this aspect as future work.

in a way to limit the interference between different UAV-SCs covering neighboring areas at the same time. In this way, when a UAV-SC covers an area, all the users in the area which were previously connected to the serving MC are handovered to the UAV-SC. We also assume that the handovers are performed in a way to limit glitches and performance losses to users. In addition, we ensure that a UAV-SC covers an area for a sufficiently long amount of time, i.e., in the order of minutes, which is much larger compared to the handover duration in 4G networks [28]. In this way, we avoid frequent handovers forced to users between the UAV-SC and the MC(s), which would otherwise impact the presented results.<sup>2</sup> In this scenario, the UAV-SC brings a throughput increase to the served area, due to the fact that: i) dedicated radio resources (in terms of BW) are allocated, ii) better channel conditions are generally experienced compared to the MCs coverage, thanks to the fact that the UAV-SC is in close proximity (i.e., at most few hundreds meters) and in Line of Sight (LoS) with the users in the area.

### 3.3 Bandwidth redistribution

A third aspect targeted by this work is the control of the BW redistribution among the terrestrial MCs when the UAV-SCs are exploited. This step involves solely the spectrum of the MCs (and no spectrum portion of the UAV-SC). When an area is served by an MC, part of the MC BW is used to provide capacity to the area. The MC BW is allocated to the area by providing radio resources to the users in the area. When the same area starts to be covered by a UAV-SC, the BW of the MC that was previously used to provide capacity over the area is then released back to the MC. Since the BW is a very precious resource for a MC, and since the UAV-SC provides a dedicated amount of BW to the area, it is meaningful to serve an area either with an MC or with a UAV-SC. Consequently, an MC does not serve any area that is being served by a UAV-SC. As a result, the MC BW is released back to the MC when the area starts to be served by the UAV-SC. In practice, the BW release is allowed by handovering the users in the area previously served by the MC to the UAV-SC currently covering the area. The released BW is then reallocated by the MC to other areas that are not served by any UAV-SC. This aspect is one of the key innovations taken into consideration by our work.

To better understand the BW redistribution, Fig. 1(a) reports a simple scenario composed of two MCs ("MC1" and "MC2"), one area exclusively served by MC1 ("Area 4"), one area exclusively served by MC2 ("Area 1"), two areas mutually served by the two MCs ("Area 2" and "Area 3"), one extra zone for delivering BW resources of MC1, and one extra zone for delivering BW resources of MC2. For simplicity, BW resources are denoted in terms of elements (represented by cubes in the subfigure), which are managed by each MC. In this scenario, Area 2 and Area 3 contain BW resources from both MCs, due to the fact that these areas are located at the coverage border for both MCs. Hence,

2. In case the TS duration is reduced (i.e. in the order of seconds or less), the impact of handovers can be carefully evaluated, e.g., by guaranteeing that each UAV-SC and each MC provide coverage over an area for at least a given number of consecutive TSs.

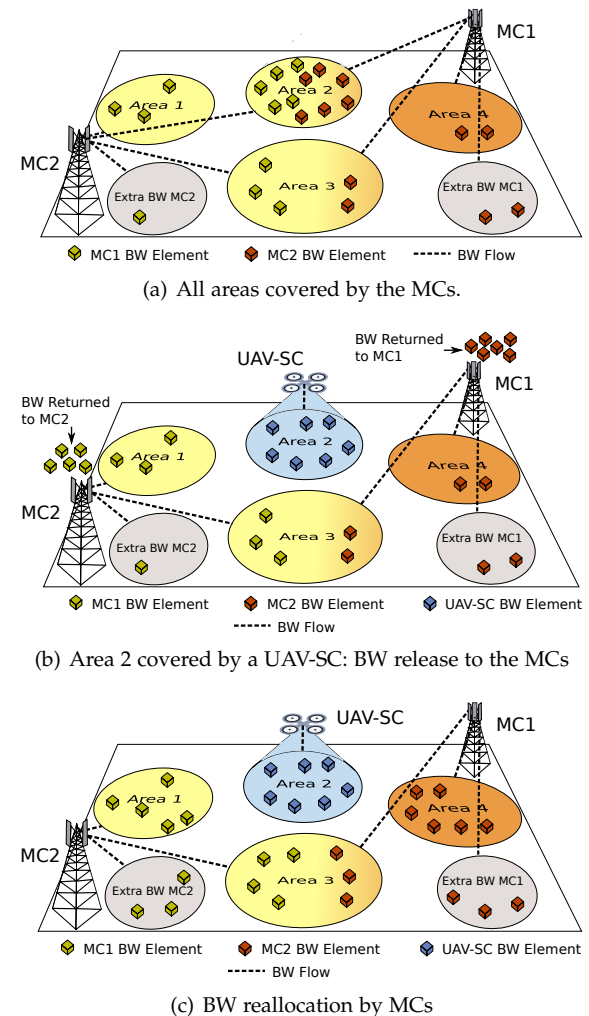


Fig. 1. MCs BW management: the BW resources assigned by MCs to Area 2 (subfigure a) are released to the MCs when Area 2 is covered by a UAV-SC (subfigure b) and they are then reallocated among the other areas not covered by UAV-SCs (subfigure c).

in order to adequately serve such areas, a large amount of BW resources of the MCs is exploited.<sup>3</sup> Now, let us suppose that Area 2 is served by a UAV-SC (Fig. 1(b)). When the SC on board the UAV starts covering the area, all the BW resources that were previously assigned to the area are released to the MCs. This pool of BW resources is then reassigned by the MCs (Fig. 1(c)) to improve the throughput of the other areas not covered by UAV-SCs (see e.g., Area 4, which passes from 2 radio resources in Fig. 1(a) to 6 radio resources in Fig. 1(c)). In this way, the exploitation of UAV-SCs allows the BW release to the MC(s) previously serving the areas, and therefore a better throughput also to the areas *not* served by any UAV-SC. This is a fundamental aspect, which was not deeply covered by the UAV-related literature so far. Without the BW redistribution, the maximization of the UAV-SC throughput would result into the maximization of the number of areas covered by UAV-SCs over time. However, the BW redistribution feature makes this objective

3. This assumption is reasonable, since users at the cell edge generally experience the worst channel conditions. Therefore, in order to guarantee a given throughput, the MC has to consume a large number of BW resources for such users.

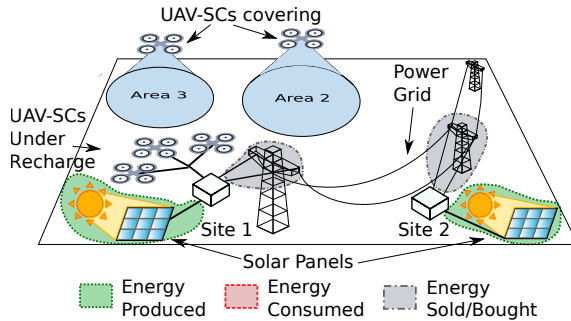


Fig. 2. Energy management at the ground sites. Each site balances the energy produced by the SPs, the energy consumed by the UAV-SCs under recharge (if any) and the energy exchanged with the grid.

not trivial. In fact, the reallocation of BW may bring, for a specific area not covered by any UAV-SC, a notable BW improvement (and consequently a throughput increase). Our work properly considers also this feature.

### 3.4 Energy management

A third aspect addressed by this work is the management of the different energy components available in the set of ground sites, as shown in Fig. 2. More specifically, each ground site hosts charging stations on which the UAV-SCs must land to recharge. The energy needed to recharge the UAV-SCs is drained from the SPs and/or the grid. Although both SPs and the grid are a source of power for the operator, we carefully distinguish them in our framework. In fact, while the energy bought from the grid has a cost for the operator, the energy from the SPs does not have a cost, as the operator is the owner of the SPs installed in each site. Moreover, the energy produced by the SPs (when it is not used to recharge the UAV-SCs) can be sold to the grid, thus realizing a revenue for the operator. In this way, the ground site balances the energy required to recharge the UAV-SCs with the energy produced by the SPs and the energy bought or sold to the grid (see e.g., Site 1 in the figure). Clearly, from an energy cost point of view, the recharge of the UAV-SCs should be minimized, in order to allow the selling of the energy produced by the SPs directly to the grid (see e.g., Site 2 in the figure).

### 3.5 UAV-SC mission scheduling

Finally, we consider the modelling of the UAV-SC missions over time and space. We assume that the time is discretized in Time Slots (TSs). The UAV-SCs missions are computed on a centralized unit, which schedules the UAV-SCs action in each TS. The communication channel between the UAV-SC and the centralized unit (which may be colocated e.g., with a MC) is assumed to be reliable. During a TS, each UAV-SC performs one of the following actions: staying parked at a ground site and not consuming any energy (STAY action), recharging at a ground site (REC), moving from a site to an area, or from an area to a site (MOV action), or covering an area (COV action).<sup>4</sup> When the COV action is selected, the UAV-SC hovers above the center of the area, with a

4. In the event that all the input parameters can be estimated in advance, the mission can be loaded on the UAV-SC during a REC or STAY action.

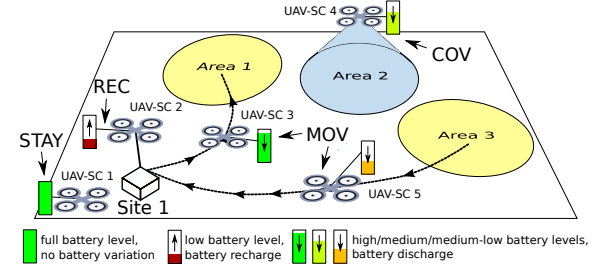


Fig. 3. UAV-SCs actions and battery levels in a sample scenario.

zero vertical/horizontal speed. In this way, the propagation conditions do not vary during a COV action.<sup>5</sup>

Fig. 3 reports a representative example showing a set of UAV-SCs, each of them performing a specific action. In this work, we precisely model the battery level of each UAV-SC, as a consequence of a given action set to a UAV-SC in a given location and at a given TS. This is also another fundamental aspect covered by this work, since the UAVs are subject to tight battery constraints [5]. More in depth, when a UAV-SC performs a REC action, its battery level is increased (see e.g., UAV-SC 2 in the figure). On the other hand, when the UAV-SC performs a MOV or a COV action, its battery level decreases. The amount of energy consumed by the MOV action depends on several parameters, like the flight path between the area and the site, the UAV-SC speed, the UAV-SC aerodynamic features and the cruise altitude, all of them taken into account by this work through a realistic energy consumption model. In addition, we assume that, when the UAV-SC performs a COV action, the SC functionalities are activated and the UAV-SC starts hovering over the area. This action is also integrated in our energy consumption model.

## 4 J-MATE FORMULATION

We formulate J-MATE in the following subsections: i) input sets and graph notation, ii) feasibility constraints, iii) objective function and complete model. The main notation introduced throughout the text is also summarized in Tab. 2.

### 4.1 Input Sets and Graph Notation

Let us denote with  $A$ ,  $S$  and  $U$  the set of areas, the set of ground sites, and the set of UAV-SCs, respectively. Without loss of generality, we assume that each site  $s \in S$  hosts MC functionalities. We denote with  $P$  the set of places, defined as  $P = A \cup S$ . We adopt the term “place” to indicate either an area or site, and consequently to simplify the problem notation.<sup>6</sup> The set of Time Slots (TSs) is denoted as  $T$ . Moreover, we denote as  $G(N, L)$  the MP graph, used to model the UAV-SCs missions over space and time. The set of nodes  $N$  of the MP graph is defined as the union of the pairs  $(p, t) \quad \forall p \in P, t \in T$ , and two fictitious nodes  $\Omega$

5. In the event that an horizontal/vertical speed is applied during a coverage action, the propagation conditions may vary. We refer the reader to the surveys presented in [29], [30] for a comprehensive overview of the effects on the propagation channel features due to the movement of the UAVs while communicating with ground stations and/or users. Clearly, such effects do not emerge in our work.

6. Without introducing the “place” notation, we would have to use separate indexes for areas and for sites, thus affecting the readability of the presented problem.

and  $\Phi$ , used to inject and collect tokens in  $G$ . We introduce the term “token” for modelling purposes, to refer to 1 unit of flow in the model J-MATE, which involves network flow optimization (see Appendix A for more details).  $L$  denotes the set of links of  $G$ , which is defined as the union of different subsets, used to model the UAV-SCs actions. Specifically, we consider movement arcs ( $L^{\text{MOV}}$ ), coverage arcs ( $L^{\text{COV}}$ ), staying arcs ( $L^{\text{STAY}}$ ) and recharging arcs ( $L^{\text{REC}}$ ) to model the MOV, COV, STAY and REC actions, respectively. Each of the aforementioned arcs is defined between node  $(p_1, t - 1)$  and  $(p_2, t)$ , where  $p_1, p_2 \in P$  and  $t \in T$ . In other words, we consider arc connections on the graph between consecutive TSs. Clearly, it holds that: i)  $p_1 \neq p_2$  for  $L^{\text{MOV}}$ , ii)  $p_1 = p_2 \in A$  for  $L^{\text{COV}}$ , iii)  $p_1 = p_2 \in S$  for  $L^{\text{STAY}}$  and  $L^{\text{REC}}$ . In addition,  $L$  includes the fictitious arcs  $L^\Omega$  and  $L^\Phi$ , which are used to move the tokens from  $\Omega$  and to  $\Phi$ , respectively. An arc  $l \in L^\Omega$  is set between  $\Omega$  and  $(p, t_{\text{START}})$ , where  $p \in P$  and  $t_{\text{START}} \in T$  is the initial TS. On the other hand, an arc  $l \in L^\Phi$  is set between  $(p, t_{\text{END}})$  and  $\Phi$ , where  $p \in P$  and  $t_{\text{END}} \in T$  is the last TS. Eventually, we denote the head  $h(l)$  of arc  $l \in L$  defined between nodes  $(p_1, t_1)$  and  $(p_2, t_2)$  as  $h(l) = (p_2, t_2)$ . In a similar way, we define the tail  $t(l)$  of arc  $l \in L$  as  $t(l) = (p_1, t_1)$ .

## 4.2 Feasibility Constraints

**Flow Constraints.** We initially introduce the binary flow variables  $m_{(l,u)}$ , which take value 1 if UAV-SC  $u \in U$  activates link  $l \in L$ , 0 otherwise. We then impose the flow conservation over the MP graph with the following constraint:

$$\sum_{\substack{l \in L: \\ t(l)=(p,t-1)}} m_{(l,u)} - \sum_{\substack{l \in L: \\ h(l)=(p,t)}} m_{(l,u)} = 0 \quad (1)$$

$$\forall p \in P, u \in U, t \in T$$

In addition, node  $\Omega$  is used to inject in the graph a single token for each UAV-SC:

$$\sum_{\substack{l \in L: \\ t(l)=\Omega}} m_{(l,u)} = 1 \quad \forall l \in L^\Omega, u \in U \quad (2)$$

Moreover, node  $\Phi$  captures the injected token for each UAV-SC through the following constraint:

$$\sum_{\substack{l \in L: \\ h(l)=\Phi}} m_{(l,u)} = 1 \quad \forall l \in L^\Phi, u \in U \quad (3)$$

By including constraints (1), (2), (3), we impose that: i) each UAV-SC may be utilized starting from the initial TS up to the final one, and ii) the mission consistency is satisfied (i.e., the UAV-SCs always perform feasible missions).

**Coverage Constraints.** We then introduce the binary variable  $c_{(a,t)}$ , which takes 1 if area  $a \in A$  is covered by one UAV-SC at TS  $t \in T$ , 0 otherwise. The value of  $c_{(a,t)}$  is set through the following equation:

$$\sum_{u \in U} \sum_{l \in L^{\text{COV}}: h(l)=(a,t)} m_{(l,u)} = c_{(a,t)} \quad \forall a \in A, t \in T : t \geq 1 \quad (4)$$

Note that the previous constraint imposes that area  $a$  is either covered by one single UAV-SC or not covered by any UAV-SC at TS  $t$ .

TABLE 2  
Main Notation.

	Symbol	Description
Sets and links notation	$A$	Set of areas
	$S$	Set of sites
	$P$	Set of places ( $P = A \cup S$ )
	$U$	Set of UAV-SCs
	$T$	Set of Time Slots (TSs)
	$\Omega, \Phi$	Source and sink nodes
	$N$	Set of nodes ( $N = (P \times T) \cup \{\Omega\} \cup \{\Phi\}$ )
	$L^{\text{MOV}}$	Set of movement (MOV) links
	$L^{\text{STAY}}$	Set of staying (STAY) links
	$L^{\text{COV}}$	Set of coverage (COV) links
Parameters	$L^{\text{REC}}$	Set of recharge (REC) links
	$L^\Omega$	Set of links from $\Omega$ node
	$L^\Phi$	Set of links to $\Phi$ node
	$L$	Set of links ( $L = L^{\text{MOV}} \cup L^{\text{STAY}} \cup L^{\text{COV}} \cup L^{\text{REC}} \cup L^\Omega \cup L^\Phi$ )
	$G(N, L)$	Multi-Period (MP) graph
	$h(l)$	Head node of link $l \in L$
	$t(l)$	Tail node of link $l \in L$
	$E_{(s,t)}^{\text{PROD}}$	Energy produced by site $s$ at TS $t \in T$
	$E_l$	Energy associated with link $l \in L$
	$W_s^{\text{TOT}}$	Total BW of MC installed in site $s \in S$
Variables	$W_{(a,s)}^{\text{BASE}}$	Baseline BW provided by MC in site $s \in S$ to area $a \in A$
	$W_a^{\text{UAV-SC}}$	BW provided by a UAV-SC to area $a \in A$
	$B^{\text{MIN}}$	Minimum UAV-SC battery level
	$B^{\text{MAX}}$	Maximum UAV-SC battery level
	$O$	Protocol overhead ( $O \in (0, 1]$ )
	$D_{(a,s)}$	Coverage matrix (1 if area $a \in A$ is covered by MC in site $s \in S$ , 0 otherwise)
	$F_{(a,s)}^{\text{MC}}$	Spectral efficiency of area $a \in A$ when served by MC in site $s \in S$
	$F_a^{\text{UAV-SC}}$	Spectral efficiency of area $a \in A$ when served by a UAV-SC
	$R^{\text{RATE}}$	Revenue for throughput
	$R_t^{\text{SELL}}$	Revenue for selling energy at TS $t \in T$
	$C_t^{\text{BUY}}$	Cost for buying energy at TS $t \in T$
Variables	$m_{(l,u)}$	Binary flow variable (1 if UAV-SC $u \in U$ activates link $l \in L$ , 0 otherwise)
	$w_{(l,u)}$	Fractional energy variable of UAV-SC $u \in U$ over link $l \in L$ ( $0 \leq w_{(l,u)} \leq 1$ )
	$c_{(a,t)}$	Binary coverage variable (1 if area $a \in A$ is covered by one single UAV-SC at TS $t \in T$ , 0 otherwise)
	$b_{(u,t)}$	Battery level variable of UAV-SC $u \in U$ in TS $t \in T$ ( $B^{\text{MIN}} \leq b_{(u,t)} \leq B^{\text{MAX}}$ )
	$e_{(s,t)}^{\text{BUY}}$	Energy bought by site $s \in S$ at TS $t \in T$ ( $e_{(s,t)}^{\text{BUY}} \geq 0$ )
	$e_{(s,t)}^{\text{SELL}}$	Energy sold by site $s \in S$ at TS $t \in T$ ( $e_{(s,t)}^{\text{SELL}} \geq 0$ )
	$g_{(a,s)}^t$	Fraction of BW released to MC in site $s \in S$ by area $a \in A$ when covered by a UAV-SC at TS $t \in T$ ( $0 \leq g_{(a,s)}^t \leq 1$ )
	$g_{(s,a)}^t$	Fraction of additional BW assigned by MC in site $s \in S$ to area $a \in A$ at TS $t \in T$ ( $0 \leq g_{(s,a)}^t \leq 1$ )
	$\gamma_s^t$	Fraction of additional BW available at MC in site $s \in S$ at TS $t \in T$ and not assigned to any area ( $0 \leq \gamma_s^t \leq 1$ )
	$r_{(a,t)}$	Downlink throughput of area $a \in A$ at TS $t \in T$ ( $r_{(a,t)} \geq 0$ )

**Energy Constraints.** We initially introduce the parameter  $E_l$  to denote the energy consumption associated with link  $l \in L$ . We then define the continuous variable  $w_{(l,u)} \in [0, 1]$  associated with link  $l \in L^{\text{REC}}$  and UAV-SC  $u \in U$ , in order to allow a partial recharge of UAV-SC battery (i.e., even lower than  $E_l$ ). In this way, the energy requested by UAV-SC  $u$  to recharge on link  $l \in L^{\text{REC}}$  is  $E_l \cdot w_{(l,u)}$ .

We then impose that  $w_{(l,u)}$  can be strictly positive iff the corresponding flow variable is activated:

$$w_{(l,u)} \leq m_{(l,u)} \quad \forall l \in L^{\text{REC}}, u \in U \quad (5)$$

In the following, we consider the energy balance implemented in the ground site. To this aim, let us denote

with  $E_{(s,t)}^{\text{PROD}}$  the energy produced by SPs installed at site  $s \in S$  during TS  $t \in T$ .  $E_{(s,t)}^{\text{PROD}}$  is an input parameter to our problem. We then introduce the continuous variables  $e_{(s,t)}^{\text{BUY}}$  and  $e_{(s,t)}^{\text{SELL}}$ , which are used to denote the amount of energy that is bought from the grid or that is sold to the grid by site  $s$  at TS  $t$ , respectively. Each site  $s$  has to balance the energy requested by the UAV-SCs under recharge, the energy produced by SPs, and the energy exchanged with the grid. More formally, we have:

$$\sum_{u \in U} E_l \cdot w_{(l,u)} - e_{(s,t)}^{\text{BUY}} + e_{(s,t)}^{\text{SELL}} = E_{(s,t)}^{\text{PROD}}$$

$$\forall l \in L^{\text{REC}} : h(l) = (s, t) \wedge t(l) = (s, t-1), s \in S, t \in T \quad (6)$$

We then introduce the  $w_{(l,u)}$  variables also for the MOV and COV link types, to make our notation homogeneous. Since fractional values of  $E_l$  are not allowed for  $L^{\text{COV}}$  and  $L^{\text{MOV}}$  (i.e., the energy consumed by the UAV-SC is equal to  $E_l$ ), we impose the following constraint:

$$w_{(l,u)} = m_{(l,u)} \quad \forall l \in L^{\text{COV}} \cup L^{\text{MOV}}, u \in U \quad (7)$$

Moreover, we model the UAV-SC battery level. We initially introduce the continuous variable  $b_{(u,t)}$  to store the battery level of UAV-SC  $u \in U$  at TS  $t \in T$ . We then compute the UAV-SC battery level as:

$$b_{(u,t)} = b_{(u,t-1)} + \sum_{\substack{l \in L^{\text{REC}} \cup L^{\text{MOV}} \cup L^{\text{COV}}: \\ t(l)=(*,t-1) \\ h(l)=(*,t)}} E_l \cdot w_{(l,u)}$$

$$\forall u \in U, t \in T \quad (8)$$

We remind that the sign of  $E_l$  values is positive for  $l \in L^{\text{REC}}$ , and negative for  $l \in L^{\text{MOV}}$  and  $l \in L^{\text{COV}}$ . In other words: a recharge action always increases the battery level, while a coverage or a movement action always decreases the battery level.

Finally, we introduce the input parameters  $B^{\text{MAX}}$  and  $B^{\text{MIN}}$  to denote the maximum and the minimum UAV-SC battery capacity, respectively. We then ensure that the UAV-SC battery level is within these bounds:

$$B^{\text{MIN}} \leq b_{(u,t)} \leq B^{\text{MAX}} \quad \forall u \in U, t \in T \quad (9)$$

**BW Redistribution Constraints.** We initially model the amount of BW released to MC located at site  $s \in S$  when a UAV-SC covers an area  $a \in A$  at TS  $t \in T$ . To this aim, we introduce the continuous variable  $g_{(a,s)}^t$  to store the fraction of BW released to MC in site  $s$  when a UAV-SC covers an area  $a$  at TS  $t$ . In addition, let us denote with  $W_s^{\text{TOT}}$  the total BW used by MC in site  $s$  and with  $W_{(a,s)}^{\text{BASE}}$  the amount of baseline BW assigned to area  $a$  by MC in site  $s$ , respectively. In addition, let us denote with  $D_{(a,s)}$  a binary matrix taking value 1 if area  $a$  can receive BW from MC in site  $s$ , 0 otherwise. Clearly, both  $W_s^{\text{TOT}}$ ,  $W_{(a,s)}^{\text{BASE}}$  and  $D_{(a,s)}$  are input parameters to our problem. The amount of BW released by area  $a$  to MC in site  $s$  at TS  $t$  is then defined as:

$$g_{(a,s)}^t = \frac{W_{(a,s)}^{\text{BASE}}}{W_s^{\text{TOT}}} \cdot D_{(a,s)} \cdot c_{(a,t)} \quad \forall a \in A, s \in S, t \in T \quad (10)$$

We then consider the amount of BW that is redistributed to areas not covered by any UAV-SC. We introduce the continuous variable  $g_{(s,a)}^t$  (having an inverse order of the

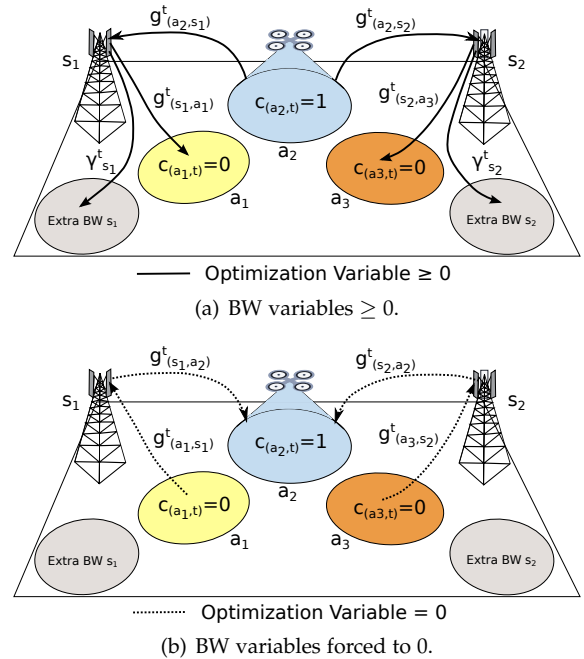


Fig. 4. BW variables in a simple scenario in which a UAV-SC covers area  $a_2$  at TS  $t$ .

indexes w.r.t.  $g_{(a,s)}^t$ ), which denotes the fraction of additional BW that is assigned to area  $a$  by MC in site  $s$ . Clearly,  $g_{(s,a)}^t$  is equal to 0 if one of the following conditions hold: i) the area  $a$  is currently covered by a UAV-SC (and hence no BW from any MC should be assigned to the area) or ii) the area  $a$  can not be covered by site  $s$  (e.g., due to the fact that it is outside the coverage of  $s$ ). Both the conditions are expressed through the following constraint:

$$g_{(s,a)}^t \leq (1 - c_{(a,t)}) \cdot D_{(a,s)} \quad \forall a \in A, s \in S, t \in T \quad (11)$$

We then consider the management of released and assigned BW at each MC. To model this aspect, we impose a flow conservation between the variables  $g_{(a,s)}^t$  and  $g_{(s,a)}^t$ . In addition, we introduce the continuous variable  $\gamma_s^t$  to store the surplus of BW that is released from (some) areas and not used to cover other areas. We recall that this surplus of BW may be used by the MC for other needs, e.g., to serve the users under mobility or other zones that are not covered at all by UAV-SCs. More formally, we have:

$$\sum_{a \in A} g_{(a,s)}^t = \sum_{a \in A} g_{(s,a)}^t + \gamma_s^t \quad \forall s \in S, t \in T \quad (12)$$

Fig. 4 reports a representative example showing how the variables  $g_{(a,s)}^t$ ,  $g_{(s,a)}^t$  and  $\gamma_s^t$  are governed by the constraints (10), (11), (12), the coverage variables  $c_{(a,t)}$  and the input matrix  $D_{(a,s)}$ . We consider a toy-case scenario composed of two MCs (installed in  $s_1$  and in  $s_2$ ) and three areas  $a_1$ ,  $a_2$  and  $a_3$ . More in depth,  $a_1$  is served by MC in  $s_1$ ,  $a_2$  is served by a UAV-SC, and  $a_3$  is served by MC in  $s_2$ . For simplicity, we report also two extra zones, used to assign extra BW apart from the one delivered to  $a_1$ ,  $a_2$  and  $a_3$ .<sup>7</sup> In this scenario, it holds that:  $c_{(a_1,t)} = 0$ ,  $c_{(a_2,t)} = 1$ ,

<sup>7</sup> An overview about the extra zones and their significance is reported in Appendix B.

$c_{(a_3,t)} = 0$ . Moreover, let us assume the following input matrix:  $D_{(a_1,s_1)} = 1$ ,  $D_{(a_1,s_2)} = 0$ ,  $D_{(a_2,s_1)} = 1$ ,  $D_{(a_2,s_2)} = 1$ ,  $D_{(a_3,s_1)} = 0$ ,  $D_{(a_3,s_2)} = 1$ . Therefore, according to (10),  $g_{(a_1,s_1)}^t = 0$ ,  $g_{(a_1,s_2)}^t = 0$ ,  $g_{(a_2,s_1)}^t \geq 0$ ,  $g_{(a_2,s_2)}^t \geq 0$ ,  $g_{(a_3,s_1)}^t = 0$ ,  $g_{(a_3,s_2)}^t = 0$ . On the other hand, according to (11),  $g_{(s_1,a_1)}^t \geq 0$ ,  $g_{(s_2,a_1)}^t = 0$ ,  $g_{(s_1,a_2)}^t = 0$ ,  $g_{(s_2,a_2)}^t = 0$ ,  $g_{(s_2,a_3)}^t \geq 0$ ,  $g_{(s_1,a_3)}^t = 0$ . Finally, according to (12) the flow  $g_{(a_2,s_1)}^t$  can be redistributed to  $g_{(s_1,a_1)}^t$  and  $\gamma_{s_1}^t$ . In a similar way, the flow  $g_{(a_2,s_2)}^t$  can be redistributed to  $g_{(s_2,a_3)}^t$  and  $\gamma_{s_2}^t$ .

**Downlink Throughput Constraints.** Let us denote a protocol overhead parameter as  $O \in (0, 1]$ . In addition, we denote by  $F_a^{\text{UAV-SC}}$  the average spectral efficiency of area  $a \in A$  when it is served by a UAV-SC. On the other hand, we denote by  $F_{(a,s)}^{\text{MC}}$  the average spectral efficiency of area  $a \in A$  when it is served by MC in site  $s \in S$ . The total throughput of area  $a$  at TS  $t \in T$  is then:

$$\begin{aligned} r_{(a,t)} = & O \cdot \left\{ F_a^{\text{UAV-SC}} \cdot W_a^{\text{UAV-SC}} \cdot c_{(a,t)} \right. \\ & \left. + \sum_{s \in S} F_{(a,s)}^{\text{MC}} \cdot \left[ W_{(a,s)}^{\text{BASE}} \cdot (1 - c_{(a,t)}) + W_s^{\text{TOT}} \cdot g_{(s,a)}^t \right] \right\} \\ & \forall a \in A, t \in T \end{aligned} \quad (13)$$

In the previous equation, we model the following options: i) the area is served by a UAV-SC, or ii) the area is served by (multiple) MCs. The coverage variable  $c_{(a,t)}$  is used to distinguish each option. In particular, if the area is covered by the UAV-SC, only the term i) is accounted. On the contrary, if the area is not served by any UAV-SC, it is served by the MC(s), which include the baseline amount of BW, plus the (possible) additional BW drained from the areas served by UAV-SCs.

### 4.3 Objective Function and Complete Model

We consider a multi-objective function to jointly pursue: i) the maximization of the revenue from traffic thanks to the exploitation of the UAV-SCs, ii) the maximization of the revenue for selling energy to the grid and iii) the minimization of the costs for buying energy from the grid. Specifically, the throughput and energy terms are properly weighed by including the following parameters: i) throughput weight  $R^{\text{RATE}}$  [NZD/Mbps] (NZD denotes the New Zealand dollar), ii) energy sold weight  $R_t^{\text{SELL}}$  [NZD/KWh], which varies over  $t \in T$ , iii) energy bought weight  $C_t^{\text{BUY}}$  [NZD/KWh], which also varies over  $t$ . The overall objective function of the JOINT MANAGEMENT OF MULTI-AREA THROUGHPUT AND ENERGY (J-MATE) model is then:

$$\max \sum_{t \in T} \left[ R^{\text{RATE}} \cdot \sum_{a \in A} r_{(a,t)} + \sum_{s \in S} R_t^{\text{SELL}} e_{(s,t)}^{\text{SELL}} - \sum_{s \in S} C_t^{\text{BUY}} e_{(s,t)}^{\text{BUY}} \right] \quad (14)$$

under constraints: (1)-(13), with variables:  $m_{(l,u)} \in \{0, 1\}$ ,  $c_{(a,t)} \in \{0, 1\}$ ,  $w_{(l,u)} \geq 0$ ,  $b_{(u,t)} \geq 0$ ,  $e_{(s,t)}^{\text{BUY}} \geq 0$ ,  $e_{(s,t)}^{\text{SELL}} \geq 0$ ,  $g_{(a,s)}^t \geq 0$ ,  $g_{(s,a)}^t \geq 0$ ,  $\gamma_s^t \geq 0$ ,  $r_{(a,t)} \geq 0$ . We also clarify that  $e_{(s,t)}^{\text{BUY}}$  and  $e_{(s,t)}^{\text{SELL}}$  are expressed in [KWh]. Moreover,  $r_{(a,t)}$  is expressed in [Mbps]. As a consequence, all the terms appearing in Eq. (14) are homogeneous, i.e., they are all expressed in [NZD].

The joint optimization is required because all the terms in Eq. (14) are deeply inter-correlated. For example, when

the energy revenues/costs are the dominant terms w.r.t. the throughput revenues ( $R^{\text{RATE}} = 0$ ), the best solution is to keep the UAV-SCs at ground in the STAY state, and sell all the energy produced by SPs to the grid. In the opposite case ( $R^{\text{RATE}} \gg 0$ ), the operator aims at maximizing the throughput revenues from users. This strategy then results in the continuous use of UAV-SCs for all the areas. Since the energy revenues/costs are much lower than the throughput revenues, the energy needed to recharge the UAV-SCs is drained from the SPs and/or from the grid. However, the two aforementioned strategies are typically in contrast, i.e. either all UAV-SCs are in the STAY state or all the UAV-SCs are continuously used. Consequently, the operator aims at studying also intermediate solutions, i.e., where a balance between energy and throughput is pursued. This balanced strategy includes also cases where the SP energy is partially sold and partially used to recharge the UAV-SCs, and/or UAV-SC coverage restricted only to specific areas (not the whole ones). Therefore, all the terms in the objective function have to be jointly evaluated with the presented approach. Our framework, in fact, is always able to maximize the joint objective function, for any value of the throughput weight  $R^{\text{RATE}}$ .

**Proposition 1.** *The J-MATE problem is NP-Hard.*

*Proof.* We consider a special case of the J-MATE, denoted as M-COV, whose goal is to maximize the coverage of the areas by means of UAV-SCs in all the TSs. M-COV is defined as:  $\max \sum_{a \in A} \sum_{t \in T} c_{(a,t)}$ , subject to: (1), (2), (3), (4) under variables:  $m_{(l,u)} \in \{0, 1\}$ ,  $c_{(a,t)} \in \{0, 1\}$ . It is possible to note that M-COV is a variant of the multi-commodity problem with unsplittable (integral) flows, a type of problem known to be NP-Hard [31]. Since M-COV is included in J-MATE, we can conclude that also J-MATE is NP-Hard.  $\square$

## 5 BBSR ALGORITHM

We develop a new algorithm, called BALANCE ENERGY BOUGHT, ENERGY SOLD AND THROUGHPUT REVENUE (BBSR) to practically solve the J-MATE problem. We report here the main steps of the algorithm, while we refer the reader to Appendix C for a detailed description (including the pseudo-codes). In brief, the main goal of BBSR is to balance the different terms in the objective function of (14), by selectively scheduling the UAV-SCs missions, the BW release, the BW assignment, and the energy that is exchanged with the grid. Compared to the J-MATE problem, the following assumptions are introduced in BBSR:

- the REC action is completed in one TS;
- each UAV-SC returns back to the site from which it started the mission;
- a pair of UAV-SCs is used to provide coverage over an area. When the first UAV-SC is covering an area, the second UAV-SC is waiting (in STAY state) on the site. During the last coverage of the first UAV-SC, the second UAV-SC moves over the area and replace the first one.

Clearly, the previous assumptions allow us to significantly reduce the problem complexity w.r.t. J-MATE formulation. However, at the same time, they allow us to fast generate

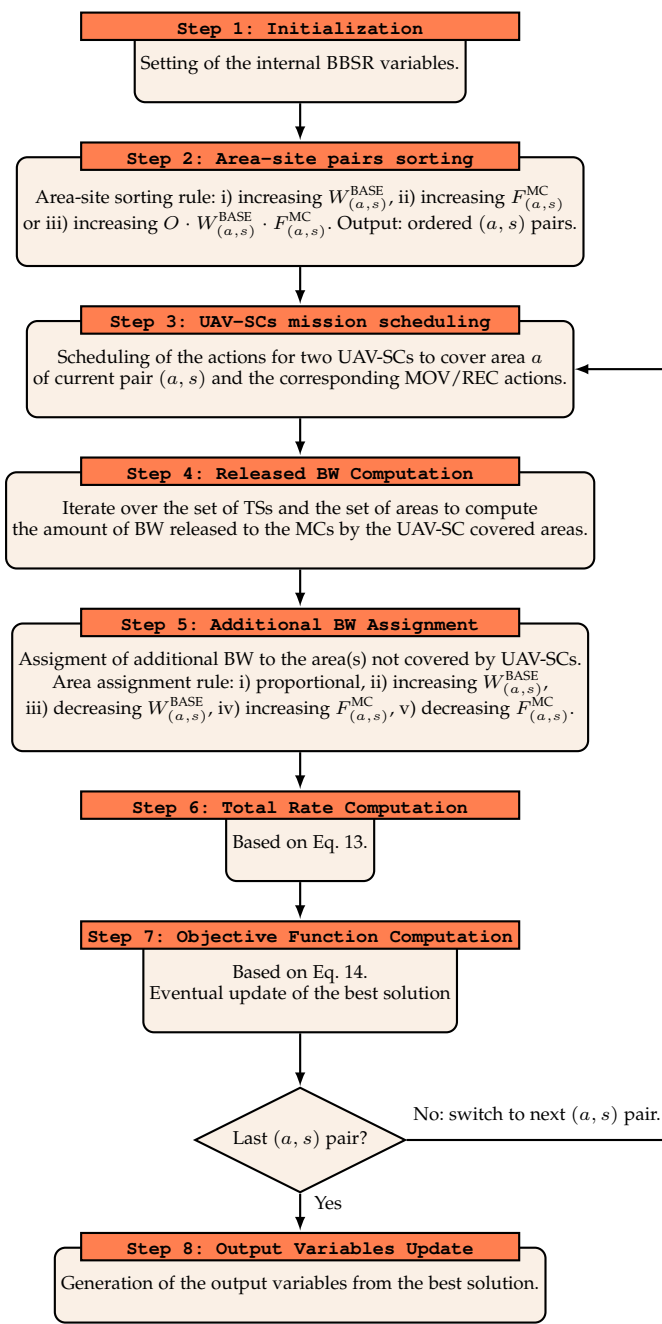


Fig. 5. High level flowchart of BBSR.

high-quality solutions that respect all the constraints of J-MATE.

Fig. 5 reports the high level flowchart of BBSR. During Step 1, BBSR initializes the internal variables, which include e.g., the value of the best objective found so far (initially set to  $-\infty$ ), the coverage of the areas (initially only provided by MCs), and the number of UAV-SCs that can be used to provide coverage (initially set to  $|U|$ ). BBSR then considers the sorting of each area-site pair  $(s, a)$  with a given rule (Step 2). The idea of this step is to prioritize the areas that need to be covered by UAV-SCs. We consider the following sorting criteria for the  $(s, a)$  pairs: i) increasing BW  $W_{(a,s)}^{\text{BASE}}$ , ii) increasing spectral efficiency  $F_{(a,s)}^{\text{MC}}$ , or iii) increasing rate  $O \cdot W_{(a,s)}^{\text{BASE}} \cdot F_{(a,s)}^{\text{MC}}$ . The selection of the sorting criterium is left

as an algorithm option. In the following (Steps 3-7), BBSR iterates over each pair  $(s, a)$ . Specifically, the algorithm schedules the missions for two UAV-SCs for the whole set of TSs in order to maximize the coverage of the current area  $a$ . This step clearly includes the setting of the REC, MOV and COV actions for the two UAV-SCs under consideration. In order to minimize the UAV-SC energy consumption, the site  $s_2$  with minimum MOV energy between  $s_2$  and  $a$  is selected as recharging place for the two UAV-SCs. Once the UAV-SCs missions are scheduled, BBSR then computes the amount of BW that is released to the MCs by the areas served with UAV-SCs (Step 4). During the following phase (Step 5), BBSR allocates the additional BW that is available on the MCs to the areas that are not covered by the UAV-SCs. To this aim, the algorithm initially orders the set of MCs with decreasing or increasing values of additional BW (the actual choice between the two options is left to the operator). Each site in the ordered list is then analyzed, in order to assign the additional BW to the areas covered by the MC. The following assignment rules are considered in order to select the area(s) that receive the additional BW: i) proportional, i.e., the additional MC BW is equally split among all the areas covered by the MC and not covered by any UAV-SC, ii) the area with lowest BW, iii) the area with highest BW, iv) the area with highest spectral efficiency, v) the area with lowest spectral efficiency. The selection of the option in use is left as a choice for the operator. In Step 6, BBSR then computes the total throughput provided to the areas by applying Eq. (13). In the following step (step 7) the objective function (14) is computed. If the objective function value of the current solution is higher than the value of the best solution found so far, the best solution is updated. Otherwise, the current solution is discarded and the changes performed during the current iteration are undone. The algorithm then passes to the next iteration (i.e., the next area-site pair). After that all the  $(s, a)$  pairs have been analyzed, the algorithm produces as output the set of variables of the best solution.

**Proposition 2.** *The computational complexity of BBSR is in the order of  $\mathcal{O}(|A| \cdot |S|^2 \cdot |T| \cdot (|A| + \log(|S|)))$ .*

*Proof.* See Appendix C. □

## 6 ROTORUA SCENARIO

We divide the description of the scenario in the following parts: i) areas, sites, and coverage level, ii) spectral efficiency and bandwidth, iii) UAV-SC energy model, iv) site energy capabilities, v) MP graph generation, and vi) number of UAV-SCs.

### 6.1 Areas, Sites and Coverage Level

We consider a rural scenario in Rotorua, a town located in the North Island of New Zealand. Fig. 6 reports the terrain view of the scenario. In order to derive realistic input parameters, we measure different metrics from a 4G network installed in Rotorua, by leveraging the CellMapper application [32] running on a Samsung S6 device and connected to the Vodafone NZ operator. We refer the reader to Appendix D for a detailed description about the collected

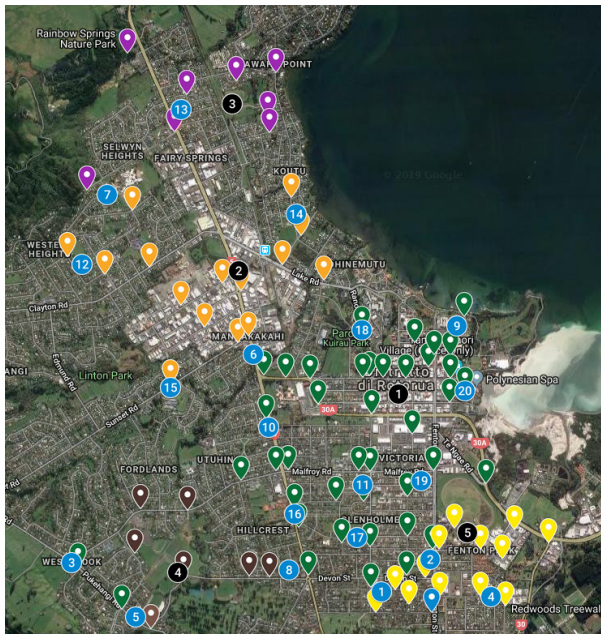


Fig. 6. Positions of MC sites (black circles), area centers (blue circles), CQI measurements (colored pins), and terrain view (source: Google Maps) in the Rotorua scenario, New Zealand. The colors of the CQI pins are set in accordance to the serving MC (Figure best viewed in colors).

metrics. In brief, we measure the current location (in GPS format), the Reference Signal Received Power (RSRP) metric, the operator's ID and the ID of the serving MC. The set of measurements taken over the territory is then used as follows. First, we extract a set of  $|S| = 5$  sites, which are assumed to be co-located with the MCs of Vodafone NZ discovered during the measurement campaign. Fig. 6 reports the geographical locations of MC sites (in black circles). As expected, the MC sites are spread over the territory to globally cover the Rotorua town. Second, we select a set of  $|A| = 20$  areas. The positions of the centers of the areas are shown in Fig. 6 with blue circles. The selection of the areas adheres to the following principles: i) avoid proximity among areas (and consequently limit the impact of interference between UAV-SCs) and ii) cover different neighborhoods of the town, where the users tend to concentrate (e.g., shopping malls, downtown buildings, recreational centers).<sup>8</sup> Third, we build the coverage map of each selected MC, given the geo-referenced RSRP values measured over the territory. Specifically, we divide the territory with a regular grid, with pixels of size equal to 500 [m]. This size is set to: i) avoid artifact coverage holes, which may appear due to the fact that our measurements are taken over the streets, and not inside courtyards, gardens and private streets, and ii) take into account that the coverage radius of a typical MC is in the order of different kilometers. For each pixel, we then count the number of RSRP measurements of the current MC site  $s \in S$  inside the pixel. If the number of measurements is zero, then the current pixel is not covered by  $s$ . Otherwise, we assume that the current pixel is covered by  $s$ . We then denote with  $\zeta_s$  [km<sup>2</sup>] the total area covered by  $s \in S$ , which is computed as the summation of the pixel

<sup>8</sup> The areas are given as input to our problem. The optimal selection of the areas is itself an NP-Hard problem. However, in our work we select the areas by adopting a heuristic (yet meaningful) approach.

areas covered by  $s$ . Fourth, we assume that the areas  $a \in A$  are circles with a radius of 250 [m] - a value in line with the coverage of currently deployed SCs [33]. We then denote the total area size as  $\zeta_a$ , which is equal to 0.19 [km<sup>2</sup>]  $\forall a \in A$ .

## 6.2 Spectral Efficiency and Bandwidth

We initially detail the steps to retrieve the spectral efficiency values. We recall that our problem requires as input: i) the spectral efficiency  $F_{(a,s)}^{\text{MC}}$  when area  $a$  is served by MC in site  $s$ , ii) the spectral efficiency  $F_a^{\text{UAV-SC}}$  when area  $a$  is served by a UAV-SC. In order to obtain the  $F_{(a,s)}^{\text{MC}}$  values, we proceed as follows: i) we measure the Channel Quality Indicator (CQI) metric at different locations over the territory, ii) we compute the average CQI from  $s$  falling in the coverage radius of  $a$ , iii) we apply the CQI - spectral efficiency conversion table of [34] to the values of i).<sup>9</sup>

Focusing on the step i), the CQI is read on the CellMapper interface after standing in the same location for a sufficiently long period of time (e.g., 2-3 minutes), to avoid side effects like fading and/or changes in the sight conditions w.r.t. the serving MC. The locations of the measurements points in the scenario are reported in Fig. 6 with colored pins, where each pin is colored in accordance to the serving MC. From the figure, we can observe that: i) the measurements are sufficiently spread over the territory, with an higher density in the town center (mid-right part of the figure), ii) CQI measurements from all the MCs in the scenario are collected. We then apply step ii) and step iii) to compute  $F_{(a,s)}^{\text{MC}}$ . The obtained values are reported in Tab. 3. Interestingly, we can note that: i) the spectral efficiency notably varies across the areas, ii) the same area is subject to different  $F_{(a,s)}^{\text{MC}}$  values when it is served by multiple MCs (see e.g., area 1 or area 2).

In the following, we compute the spectral efficiency when the area is served by a UAV-SC. To this aim, we set  $F_a^{\text{UAV-SC}} = 3.9$  [bps/Hz]. We refer the reader to Appendix E, which provides more insights about this setting. In brief, the selected value corresponds to the maximum efficiency, which is assumed to be achieved due to the good channel conditions experienced by the users in the area (i.e., Line of Sight and proximity to the SC).

In the next part, we compute the values of baseline BW assigned by each MC to each area. By assuming a fair BW assignment among the MCs serving the same area  $a$ , the baseline BW provided to area  $a$  by MC in site  $s$  is computed as:

$$W_{(a,s)}^{\text{BASE}} = W_s^{\text{TOT}} \cdot \frac{\zeta_a}{\eta_a \cdot \zeta_s} \quad (15)$$

where  $W_s^{\text{TOT}} = 20$  [MHz] (i.e., a typical setting for an MC),  $\zeta_a$  is the area size,  $\eta_a$  is the number of MCs serving  $a$ , and  $\zeta_s$  is the total portion of territory covered by MC in site  $s$ . The obtained values of  $W_{(a,s)}^{\text{BASE}}$  are reported in Tab. 4. By observing the values in the table, a strong heterogeneity of  $W_{(a,s)}^{\text{BASE}}$  values emerges across the areas, and even across the different MCs serving the same area. In any case, the values of baseline BW are not very large (i.e., much lower compared to the entire MC BW  $W_s^{\text{TOT}}$ ), thus suggesting that

<sup>9</sup> In case of non integer average CQI values, we apply a weighted average between upper and lower integer numbers.

TABLE 3  
Area spectral efficiency  $F_{(a,s)}^{\text{MC}}$  [bps/Hz] - Rotorua Scenario.

	Area ID																				
	1	2	3	4	5	6	7	8	9	10	11	12	13	14	15	16	17	18	19	20	
Site ID	1	0.6	2.3	1.7	-	1.7	-	-	0.4	2.7	0.8	1.9	-	-	-	-	2.1	1.2	0.2	1.3	1.8
	2	-	-	-	-	-	1.9	-	-	-	-	-	2.3	-	1.7	1.3	-	-	-	-	-
	3	-	-	-	-	-	-	2.3	-	-	-	-	0.2	-	-	-	-	-	-	-	-
	4	-	-	-	-	1.9	-	-	2.7	-	-	-	-	-	-	-	-	-	-	-	-
	5	1.5	1.9	-	1.7	-	-	-	-	-	-	-	-	-	-	-	-	-	-	-	-

TABLE 4  
Baseline BW  $W_{(a,s)}^{\text{BASE}}$  [MHz] for each site and each area in the Rotorua Scenario.

	Area ID																			
	1	2	3	4	5	6	7	8	9	10	11	12	13	14	15	16	17	18	19	20
Site ID	1	0.3	0.3	0.6	-	0.3	-	-	0.3	0.6	0.6	0.6	-	-	-	0.6	0.6	0.6	0.6	0.6
	2	-	-	-	-	-	0.7	-	-	-	-	0.7	-	0.7	0.7	-	-	-	-	-
	3	-	-	-	-	-	-	1.4	-	-	-	-	-	1.4	-	-	-	-	-	-
	4	-	-	-	-	0.9	-	-	0.9	-	-	-	-	-	-	-	-	-	-	-
	5	0.9	0.9	-	1.8	-	-	-	-	-	-	-	-	-	-	-	-	-	-	-

there is ample room to improve the throughput thanks to the exploitation of the UAV-SCs. Eventually, the impact of increasing the amount of MC BW provided to each area is discussed in Appendix F.

In the following, we set the amount of BW provided by UAV-SC to  $W_a^{\text{UAV-SC}} = 5$  [MHz], i.e. a typical BW setting for a small cell.<sup>10</sup> Although the MC manages a larger amount of BW compared to a UAV-SC, we stress the fact that  $W_s^{\text{TOT}}$  is divided across the areas (in accordance to Eq. 15). Consequently, the total BW over the area from the MCs  $\sum_s W_{(a,s)}^{\text{BASE}}$  is much lower compared to the UAV-SC BW  $W_a^{\text{UAV-SC}}$ , even when an area is served by multiple MCs. For example, let us consider Area 1 in Tab. 4: this area achieves  $W_a^{\text{UAV-SC}} = 5$  [MHz] when served by a UAV-SC and only  $\sum_s W_{(a,s)}^{\text{BASE}} = 1.2$  [MHz] of BW when served by the MCs.

Finally, the protocol overhead  $O$  is set equal to 0.64, in accordance to [34].

### 6.3 UAV-SC energy model

In order to compute the UAV-SC energy consumption, we start from the energy model of [27], which takes already into account several important energy terms. In this way, we model: i) the amount of energy that is spent by the UAV-SC on the horizontal component (i.e., the level flight energy consumption), including the energy due to hovering, ii) the amount of energy that is spent by the UAV-SC on the vertical component (i.e., climbing/descending energy consumption). The model of [27] is based on the aerodynamical equations of [35], which are retrieved by assuming that the UAV-SC is in a quasi-static equilibrium condition, i.e., the UAV-SC moves smoothly with a small acceleration/deceleration and the cruising speed is almost constant during each TS. Under such hypothesis, the impact of accelerations/decelerations on the energy consumption can be neglected. This assumption is reasonable in our work since: i) the adopted TS duration is much larger compared

10. Telecom Italia Mobile (TIM), one of the largest operators in Italy, exploits a bandwidth of 20 [MHz] at the 1800 [MHz] frequency, and 5 [MHz] at the 2100 [MHz] frequency. In line with this setting, each MC and each UAV-SC can allocate up to 20 [MHz] and 5 [MHz], respectively. As a result, the MCs and the UAV-SCs operate on separate portions of the radio spectrum and on distinct frequencies that do not interfere with each other.

to the accelerating/decelerating instants, ii) we adopted a low speed for the UAV-SC (equal at most to 2.66 [m/s] in our scenario), iii) we validate the energy model in a realistic testbed, showing a good matching between the predicted energy consumption and the measured one. In addition to [27], we introduce the energy consumption due to the activation of SC functionalities by the UAV-SC during the area coverage.

More formally, we recall that the energy consumption  $E_l$  is a weight associated with link  $l \in L$  of the MP graph, which is computed as the summation of the different energy components, depending on the action associated with  $l$ , i.e. MOV, COV, STAY, REC. Let us denote with  $E_l^F$ ,  $E_l^V$ ,  $E_l^{\text{SC}}$  the level flight energy consumption, the climbing/descending energy consumption, and the SC energy consumption, respectively. When the UAV-SC performs a MOV action on link  $l$ , a change on the vertical/horizontal component is enforced. Consequently, the total energy consumption  $E_l$  is:

$$E_l = E_l^F + E_l^V, \quad \forall l \in L^{\text{MOV}} \quad (16)$$

On the other hand, when the UAV-SC performs a COV action on link  $l$ , the UAV-SC hovers over the area and it activates the SC functionalities. In this case,  $E_l$  is expressed as:

$$E_l = E_l^F + E_l^{\text{SC}}, \quad \forall l \in L^{\text{COV}} \quad (17)$$

Focusing then on the energy consumption associated to STAY actions, we assume that no energy is consumed when the UAV-SC is parked in a ground site. In a similar way, the activation of the links from/to the fictitious nodes  $\Omega$  and  $\Phi$  does not vary the UAV-SC energy. More formally, we have:  $E_l = 0 \quad \forall l \in \{L^{\text{STAY}} \cup L^\Omega \cup L^\Phi\}$ . Focusing on REC actions, we set  $E_l = 1000$  [Wh]  $\forall l \in L^{\text{REC}}$ ,  $B^{\text{MAX}}=1000$  [Wh],  $B^{\text{MIN}}=100$  [Wh], as in [12].

In the following, we formally denote  $E_l^F$  and  $E_l^V$  by leveraging the model of [27]. Specifically, the level flight energy consumption  $E_l^F$  is defined as:

$$E_l^F = \frac{(m \cdot g)^2}{\sqrt{2}\delta \cdot \sigma} \frac{1}{\sqrt{H_l^{(2)} + \sqrt{H_l^{(4)} + (\frac{m \cdot g}{\delta \cdot \sigma})^2}}} \Delta_t, \quad l \in L^{\text{MOV}} \cup L^{\text{COV}} \quad (18)$$

where  $m$ ,  $g$ ,  $\delta$ ,  $\sigma$  and  $\Delta_t$  are the UAV-SC mass, the gravitational acceleration, the air density, the area of the UAV-SC

rotor disks and the TS duration, respectively. In addition,  $H_l$  denotes the horizontal speed, which is computed as:

$$H_l = \frac{\epsilon_{(p_1, p_2)}}{\Delta_t}, \forall l : h(l) = (p_2, t), t(l) = (p_1, t) \quad (19)$$

where  $\epsilon_{(p_1, p_2)}$  is the distance between place  $p_1$  and place  $p_2$ .<sup>11</sup> In our scenario, we adopt the following settings:  $m = 12$  [kg],  $g = 9.81$  [m/s<sup>2</sup>],  $\delta = 1.225$  [kg/m<sup>3</sup>]<sup>12</sup> [27],  $\sigma = 3.141$  [m<sup>2</sup>],<sup>12</sup>  $\epsilon_{(p_1, p_2)}$  based on the real positions of the places shown in Fig. 6, and  $\Delta_t = 600$  [s]  $\forall t \in T$ . Moreover, when the UAV-SC performs a COV action, it hovers over the center of area  $a$ . In this condition, it holds that  $H_l = 0$ ,  $\forall l \in L^{COV}$ .

We then consider the climbing/descending energy consumption  $E_l^V$ , which is defined as:

$$E_l^V = m \cdot g \cdot V_l \cdot \Delta_t, \quad l \in L^{MOV} \quad (20)$$

where  $V_l$  is the vertical speed on link  $l$ . If the UAV-SC is climbing, then  $V_l \geq 0$ . Otherwise, if the UAV-SC is descending,  $V_l \leq 0$ . In our scenario, the UAV-SC climbs from the ground level to the cruise altitude when performing a MOV action from a site to an area. On the contrary, the UAV-SC descends from the cruise altitude to the ground level when performing a MOV action from an area to a site.  $V_l$  is then formally expressed as:

$$V_l = \begin{cases} \frac{\kappa}{\Delta_t} & \text{if } l \in L^{MOV}, p_1 \in S, p_2 \in A, \\ -\frac{\kappa}{\Delta_t} & \text{if } l \in L^{MOV}, p_1 \in A, p_2 \in S, \end{cases} \quad (21)$$

where  $(p_1, t_1) = t(l)$ ,  $(p_2, t_2) = h(l)$ ,  $t_1 = (t-1)$ ,  $t_2 = t$ ,  $\kappa = 200$  [m] is the cruise altitude, which is again set in accordance to a typical UAV-SC setting [5].

Eventually, we introduce the SC energy consumption  $E_l^{SC}$ , which is expressed as:

$$E_l^{SC} = P_t^{SC} \cdot \Delta_t, \quad \forall l \in L^{COV} \quad (22)$$

where  $P_t^{SC} = 200$  [W] is the power consumed by SC functionalities, chosen in accordance to a realistic setting (see e.g., [36] with one transmission node).

Finally, we validated the considered model in a realistic testbed adopting a real UAV. We refer the reader to Appendix H for the details. In brief, we find a good matching between the energy values computed through the considered model and the real ones measured in the testbed.

#### 6.4 Site Energy Capabilities

We initially set the SP energy production in each site  $E_{(s,t)}^{PROD}$ . To this aim, we assume an SP plant of size equal to 10 [kWp] deployed in each site. Moreover, we consider  $|T|=144$  TSs over 24h, resulting in  $\Delta_t = 600$  [s].<sup>13</sup> In addition, we select one day in December (corresponding to the summer in the Southern hemisphere). We then plug the day, the position location, the size of the SP plant and the day in the PVWatts calculator [37] to obtain the SP energy production over time

11. The impact of distance in Eq. (18) and Eq. (19) is thoroughly analyzed in Appendix G.

12. With this setting, a rotor disk of diameter equal to 2 [m] is assumed.

13. This setting is in accordance with the  $\Delta_t$  values used in the UAV-SC energy model of Sec. 6.3. A discussion about the impact of TS duration is reported in Appendix I.

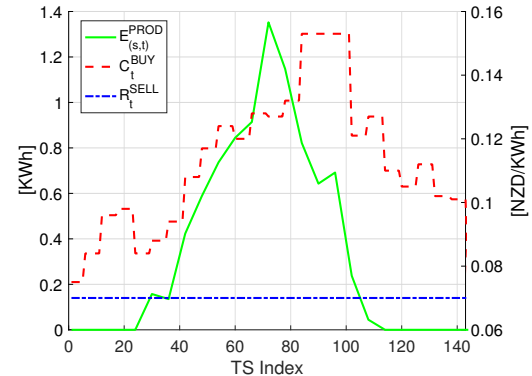


Fig. 7. Energy produced vs. time  $E_{(s,t)}^{PROD}$  [KWh] for each site  $s \in S$ , revenue from the energy sold vs. time  $R_t^{SELL}$  [NZD/KWh], and cost for the energy bought vs. time  $C_t^{BUY}$  [NZD/KWh].

$E_{(s,t)}^{PROD}$ . Without loss of generality, we assume the same trend of  $E_{(s,t)}^{PROD}$  for all the sites  $s \in S$ . The obtained values of  $E_{(s,t)}^{PROD}$  are then shown in Fig. 7. As expected, the energy production is positive during the day and zero during the night.

In the following, we consider the setting of the revenue from the energy sold  $R_t^{SELL}$ , which is set equal to 0.07 [NZD/KWh]  $\forall t \in T$  in accordance to [38]. We then set the cost for the energy bought  $C_t^{BUY}$  from the NZ electricity authority [39]. By observing the trends of  $R_t^{SELL}$  and  $C_t^{BUY}$ , reported in Fig. 7, we can note that  $C_t^{BUY} > R_t^{SELL} \forall t \in T$  (as expected).

#### 6.5 Multi-Period Graph Generation

We take into account the steps to generate the MP graph  $G(N, L)$ , which is used to model the UAV-SC missions over space and time. The nodes  $N$  are the pairs  $(p, t)$  where  $p \in S \cup A$  and  $t \in T$ . In addition, we add to  $N$  the fictitious nodes  $\Omega$  and  $\Phi$ . Focusing on the links  $l \in L$ , the energy of each link  $E_l$  is set in accordance to the link type ( $L^{MOV}$ ,  $L^{COV}$ ,  $L^{REC}$ ,  $L^{STAY}$ ,  $L^\Omega$ ,  $L^\Phi$ ), as detailed in Sec. 6.3. Moreover, in order to prevent an excessive number of links in  $G$ , we prune the original graph by removing all the links between two places  $p_1$  and  $p_2$  meeting one of the following criteria: i) distance  $\epsilon_{(p_1, p_2)} > 1600$  [m] and ii)  $p_1 = s_1 \in S$ ,  $p_2 = s_2 \in S$ ,  $s_1 \neq s_2$ , iii)  $p_1 = a_1 \in A$ ,  $p_2 = a_2 \in A$ ,  $a_1 \neq a_2$ . In this way, i) we avoid an excessive distance travelled by a UAV-SC from a site to an area, ii) a UAV-SC serving an area has to come back to a site before serving another area (while the serving of the same area across a set of consecutive TSs is allowed), and iii) when moving from a site to (another) one, at least one area has to be visited during the mission. The resulting graph is then composed of  $|N| = 3602$  nodes and  $|L| = 16456$  links.

#### 6.6 Number of UAV-SCs

We set the number of UAV-SCs equal to the double of the number of areas, i.e.  $|U| = 2 \cdot |A| = 40$ . In this way, we guarantee that each area can be potentially covered by a UAV-SC in each TS, given the considered set of input parameters. At the same time, through this setting we avoid an excessive number of UAV-SCs, which would otherwise increase too

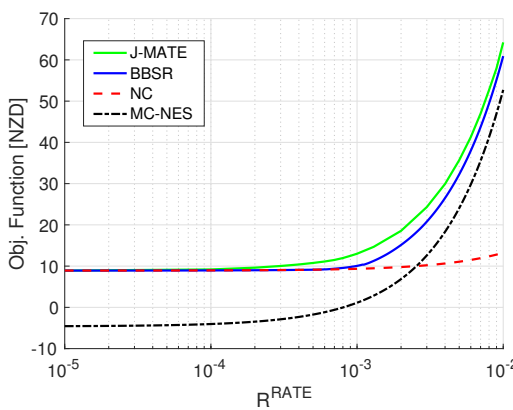


Fig. 8. Objective function variation for J-MATE, BBSR, NC and MC-NES vs. the throughput revenue  $R^{\text{RATE}}$  ( $|T| = 24$ ).

much the number of flow variables  $m_{(l,u)}$  appearing in the J-MATE formulation. The impact of varying the number UAV-SCs is discussed in Appendix J.

## 7 RESULTS

We code the J-MATE model as a C++ program, which is run by CPLEX v12.8 on a server machine equipped with a 3.5 [GHz] Xeon 8-Cores CPU and 64 [GB] of RAM. The BBSR algorithm is coded in Matlab and run on the same server machine with the software Matlab 2017. We also consider the following stopping criteria for the optimization of J-MATE: i) a maximum time limit of 24 [hours], and ii) a MIP gap tolerance  $\leq 2\%$ . In this way, J-MATE returns the current solution if either condition i) or ii) is verified. Focusing on BBSR, we set the following algorithm parameters: area-site pairs sorted by increasing  $W_{(a,s)}^{\text{BASE}}$  values, site sorting based on decreasing additional BW, additional BW assigned with a proportional rule.<sup>14</sup> We then run the J-MATE model and the BBSR algorithm over the Rotorua scenario. In order to add two terms of comparison, we consider the following strategies: i) MAXIMUM UAV-SC COVERAGE - NO ENERGY SOLD (MC-NES), which targets the maximization of the areas covered by the UAV-SCs over the set of TSs, without selling any energy to the grid, and ii) NO UAV-SC COVERAGE (NC), which instead always assumes that the areas are served solely by the MCs. In this way, all the UAV-SCs are always in the STAY state and the whole energy produced by SPs is sold to the grid using this strategy. We refer the reader to Appendix K for a formal description of MC-NES and NC.

### 7.1 Objective Function Variation

Since running J-MATE with  $|T| = 144$  TSs is computationally infeasible (due to the size of the problem and its NP-Hardness nature), we consider a subset of  $|T| = 24$  TSs, from  $t_1=61$  to  $t_2=84$ , i.e., the central hours of SP energy production in Fig. 7. We then run J-MATE, BBSR, MC-NES and NC over the set of 24 TSs. Fig. 8 reports the values of the

14. The selected combination of parameters achieved the best performance compared to the other possible ones (not reported here due to the lack of space.)

TABLE 5  
Computational comparison of J-MATE and BBSR ( $|T| = 24$ ).

	Metric	$R^{\text{RATE}}$ [NZD/Mbps]			
		$10^{-5}$	$10^{-4}$	$10^{-3}$	$10^{-2}$
J-MATE	Time	6.19 [s]	774.71 [s]	62278.57 [s]	60192.36 [s]
	Memory	N.A.	288.26 [MB]	67765.89 [MB]	8431.71 [MB]
	MIP gap	0.46%	1.91%	5.15%	1.91%
BBSR	Time	< 1 [s]			
	Memory	0.44 [MB]			

objective function of Eq. (14), which is produced as output by J-MATE, BBSR, and computed with a post-processing step with MC-NES and NC. The figure reports the value of the objective function by varying the throughput weight  $R^{\text{RATE}}$ , which we remind is a key parameter completely managed by the operator. On the contrary, the other input parameters appearing in Eq. (14), namely  $R_t^{\text{SELL}}$  and  $C_t^{\text{BUY}}$ , are not managed by the operator: both of them are set in accordance to the real energy market values shown in Fig. 7, for the considered TS interval. By analyzing in more detail Fig. 8, when  $R^{\text{RATE}}$  is low (left part of the figure), there is no revenue from serving the areas with the UAV-SCs. Consequently, no UAV-SC is used by J-MATE and BBSR. In this case, all the energy is sold to the grid, thus realizing a revenue for the operator. The obtained gain is the maximum one since the two strategies overlap with NC. On the other hand, the MC-NES strategy introduces a cost loss in this case, since maximizing the UAV-SC coverage has a negative impact on the objective function. When the throughput  $R^{\text{RATE}}$  is increased (from left to right part of the figure), we can see that all the strategies tend to increase the objective function (as expected). However, the best strategy turns out to be J-MATE, which takes explicitly into account all the revenues/costs terms. In addition, BBSR performs pretty close to J-MATE. Clearly, for large values of  $R^{\text{RATE}}$  (right part of the figure), the NC strategy turns out to be the worse one. This is an expected result, as in this case serving an area with a UAV-SC brings a substantial increase in the throughput, and hence an increase in the objective function. Since NC does not exploit any UAV-SC, the gap compared to the other strategies is very large. Overall, the results confirm that J-MATE and BBSR are always able to achieve the best solutions in terms of objective function, for any given value of  $R^{\text{RATE}}$ . This is an important outcome, as the actual value of  $R^{\text{RATE}}$  is chosen by the operator, based on its policies, e.g., maximizing the throughput revenues, minimizing the energy costs, or a mixture between the previous two terms.

### 7.2 Computational Performance

In the following, we describe the computational metrics considered to evaluate the performance of J-MATE and BBSR. Focusing on J-MATE, we consider: i) the time to retrieve the best solution, ii) the virtual memory occupation (reported by CPLEX), and iii) the MIP gap of the best solution found. Focusing on BBSR, we take into account: i) the time to run the algorithm, and ii) the virtual memory occupation (reported by Matlab). Tab. 5 reports the obtained results vs. a set of representative values of  $R^{\text{RATE}}$ . Several considerations

TABLE 6  
Performance Metrics.

Metric	Expression
Total Data Rate	$\rho^{\text{TOT}} = \sum_{t \in T} \sum_{a \in A} r(a, t)$
Energy Balance	$B^{\text{ENERGY}} = \sum_{t \in T} \sum_{s \in S} (R_t^{\text{SELL}} e_{(s,t)}^{\text{SELL}} - C_t^{\text{BUY}} e_{(s,t)}^{\text{BUY}})$
Rate Fairness	$J^{\text{RATE}} = \frac{(\sum_{a \in A} \hat{r}_a)^2}{( A  \cdot \sum_{a \in A} \hat{r}_a^2)}$ $\hat{r}_a = \frac{\sum_{t \in T} r(a, t)}{ T }$
Gain on Energy Sold	$G^{\text{SELL}} = \frac{\sum_{s \in S} \sum_{t \in T} e_{(s,t)}^{\text{SELL}}}{\sum_{s \in S} \sum_{t \in T} E_{(s,t)}^{\text{PROD}}}$
Saving on Energy Bought	$S^{\text{BUY}} = 1 - \frac{\sum_{s \in S} \sum_{t \in T} e_{(s,t)}^{\text{BUY}}}{E_{MC-NES}^{\text{BUY}}}$
Rate Fraction	$F^{\text{RATE}} = \frac{\rho^{\text{TOT}}}{\sum_{a \in A}  T  \cdot O \cdot F_a^U AV - SC \cdot W_a^U AV - SC}$
Released BW	$W^{\text{REL}} = \sum_{s \in S} \sum_{a \in A} \sum_{t \in T} W_s^{\text{TOT}} \cdot g_{(a,s)}^t$
Assigned BW	$W^{\text{AS}} = \sum_{s \in S} \sum_{a \in A} \sum_{t \in T} W_s^{\text{TOT}} \cdot g_{(a,s)}^t$

hold in this case. First, when  $R^{\text{RATE}}$  is low (left part of the table), solving the optimization problem is in general easy, as the best solution does not exploit UAV-SCs. Second, when  $R^{\text{RATE}}$  is increased, the problem starts exploiting the UAV-SCs to cover areas. Consequently, we can note a huge increase of the considered metrics (time, memory and mip-gap). Third, when  $R^{\text{RATE}}$  assumes the intermediate value of  $10^{-3}$  [NZD/Mbps], the problem is even more challenging to be solved, since all the virtual memory available by the server is occupied, and the program has to be manually stopped. Fourth, when  $R^{\text{RATE}}$  is further increased (right part of the table), J-MATE still requires large resources to be solved. Focusing instead on BBSR, both the time to retrieve the solution and the memory occupation are always very low, thus proving the computational efficiency of our heuristic. Moreover, the metrics are not affected by the variation of  $R^{\text{RATE}}$ . This is an expected result, as  $R^{\text{RATE}}$  does not influence the algorithm complexity (reported in Sec. 5).

### 7.3 Rate, Energy, and Fairness Comparison

We then consider the full set of TSs  $|T| = 144$  and we run the BBSR, MC-NES and NC algorithms. We perform an investigation of the impact of the weight  $R^{\text{RATE}}$  under a set of performance metrics. More in depth, we initially consider: i) the total data rate (denoted as  $\rho^{\text{TOT}}$ ), ii) the balance between the energy revenues and the energy costs (denoted as  $B^{\text{ENERGY}}$ ), iii) the Jain's fairness index on the average rate per area over time (denoted as  $J^{\text{RATE}}$ ). The equations to compute  $\rho^{\text{TOT}}$ ,  $B^{\text{ENERGY}}$  and  $J^{\text{RATE}}$  are detailed in Tab. 6. Fig. 9(a) reports  $\rho^{\text{TOT}}$  for the different strategies. As expected, the lower bound on  $\rho^{\text{TOT}}$  is achieved by NC, since this strategy does not use any UAV-SC. On the other hand, the upper bound is achieved by MC-NES, thanks to the coverage provided by the UAV-SCs over the areas. In addition, the ratio between upper and lower bound is more than one order of magnitude, since each UAV-SC covering an area introduces a joint increase of spectral efficiency and BW. Interestingly, BBSR presents an increasing trend between lower and upper bounds, depending on the values of  $R^{\text{RATE}}$ .

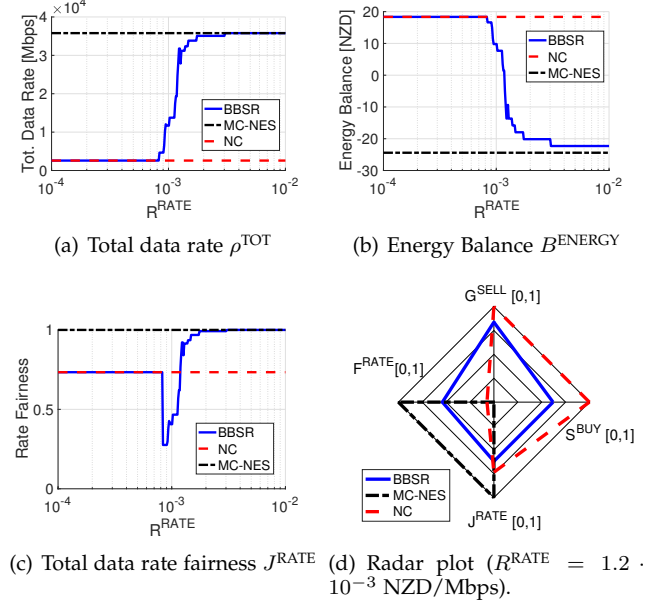


Fig. 9. BBSR, NC and MC-NES comparison ( $|T| = 144$ ).

Fig. 9(b) reports then the values of  $B^{\text{ENERGY}}$ . In this case, we can observe an inverse trend compared to  $\rho^{\text{TOT}}$ . Specifically, the best strategy is now NC, which sells all the energy produced by SPs to the grid. The MC-NES strategy requires instead an amount of energy bought from the grid, and therefore  $B^{\text{ENERGY}} < 0$ . Again, BBSR is able to adapt between the two aforementioned conditions. Finally, the  $J^{\text{RATE}}$  metric is shown in Fig. 9(c). Three consideration hold: i)  $J^{\text{RATE}}$  is maximum with MC-NES, due to the fact that all the areas receive the same throughput, thanks to the UAV-SC coverage; ii) the fairness of NC is lower than the one of MC-NES, since the area throughput for this strategy is computed solely from the MC spectral efficiency and MC baseline BW, which strongly vary in our scenario (see Tab. 3-4); iii) the fairness of BBSR is equal to NC when no UAV-SC is exploited, then lower than NC when (few) UAV-SCs are exploited, and rapidly approaching the fairness of MC-NES when a large number of UAV-SCs is used to cover the areas.

In the following, we consider an additional set of metrics in the range  $[0, 1]$  to better position BBSR, MC-NES and NC. More in depth, we take into account: i) the gain from the energy sold  $G^{\text{SELL}}$ , ii) the saving on the energy bought  $S^{\text{BUY}}$ , iii) the fraction of data rate  $F^{\text{RATE}}$ , and iv) the already introduced fairness index on the rate  $J^{\text{RATE}}$ . All the metrics are expanded in Tab. 6. Focusing on the expression of  $S^{\text{BUY}}$ , the denominator  $E_{MC-NES}^{\text{BUY}}$  is the total energy bought by the MC-NES strategy. Focusing instead on the expression of  $F^{\text{RATE}}$ , the denominator in this case is the total throughput achieved when the UAV-SCs covers all the areas in all the TSs. Fig. 9(d) reports the radar plot with the four considered metrics and the different strategies. In general, the radar plot is useful in scenarios where the comparison of the algorithms integrates several metrics, each of them normalized between 0 and 1, where 0 is the worst value and 1 is the best one. The metric value of a given algorithm is then mapped on an axis. The connection of the points over the different axes for a given algorithm

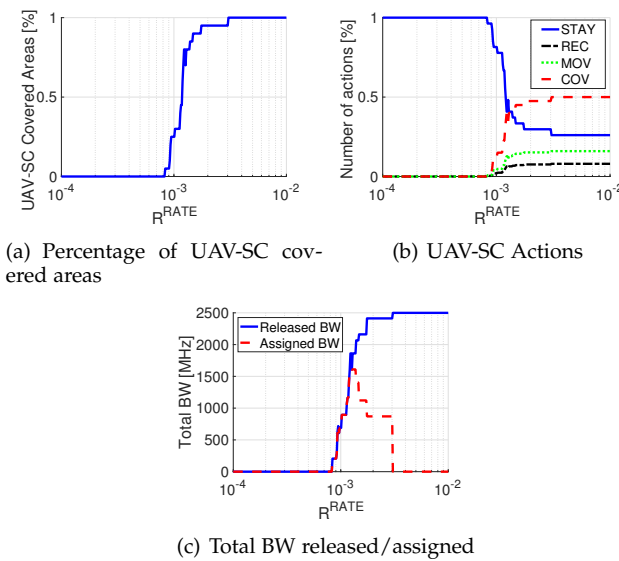


Fig. 10. UAV-SCs actions, percentage of areas covered by UAV-SCs and total BW released/assigned vs.  $R^{RATE}$  variation for BBSR ( $|T| = 144$ ).

delimits a polygon. In our case, the coordinates of the points are given by the values of the metrics in the following order (counter-wise from top):  $(0, G^{SELL})$ ,  $(S^{BUY}, 0)$ ,  $(0, -J^{RATE})$  and  $(-F^{RATE}, 0)$ . In addition, we consider the output of BBSR by setting an intermediate value of the throughput weight  $R^{RATE} = 1.2 \cdot 10^{-3}$  [NZD/Mbps]. By observing the shape, the size and the position of the polygon in the radar plot, it is possible to obtain fruitful indications about the global performance achieved by the algorithm over the different metrics. For example, when the polygon is not centered at the origin, its shape is irregular, and the covered area is small, the considered algorithm is unbalanced among the different metrics. In our case, this behaviour clearly emerges for NC, which is more oriented in maximizing  $G^{SELL}$  and  $S^{BUY}$ , rather than  $F^{RATE}$  and  $J^{RATE}$ . On the other hand, an opposite trend occurs for MC-NES, which tends to solely maximize  $F^{RATE}$  and  $J^{RATE}$ . Interestingly, the polygon of BBSR is centered at the origin of the axes, its shape is pretty regular and its area covers almost all the axes. Consequently, BBSR is able to perform well under the different metrics.

#### 7.4 BBSR Analysis

We now evaluate the performance of BBSR in more detail. Fig. 10(a) reports the percentage of served areas (computed across all the areas and all the TSs) vs. the variation of  $R^{RATE}$ . Interestingly, BBSR is able to pass from 0% to 100% of areas covered by UAV-SCs, depending on the  $R^{RATE}$  values. We then move our attention to the different actions performed by the UAV-SCs (i.e., STAY, MOV, COV and REC). Fig. 10(b) reports the percentage of actions vs.  $R^{RATE}$ . When  $R^{RATE}$  is low (left part of the figure), all the UAV-SCs are in the STAY state, i.e., parked at the ground sites and not consuming energy. Then, as soon as  $R^{RATE}$  is increased, the COV, MOV and REC actions start to be applied. At last, for large values of  $R^{RATE}$  (right part of the figure), half of the actions belong to the COV category. This is an expected result, since, with

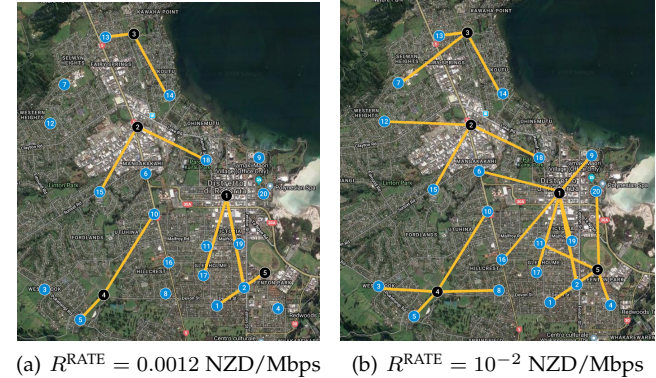


Fig. 11. UAV-SCs paths set by BBSR (Subfigures best viewed in colors).

this setting, half of the UAV-SCs are covering the areas, and half are doing other actions.<sup>15</sup>

In the following, we consider the total amount of BW released by the areas to the sites  $W^{REL}$  and the total amount of BW assigned by the sites to the areas  $W^{AS}$ . The formal expressions of  $W^{REL}$  and  $W^{AS}$  are detailed in Tab. 6, while the values w.r.t.  $R^{RATE}$  variation are shown in Fig. 10(c). We remind that the  $W^{REL}$  is the total amount of MC BW released to the MCs by the areas covered by UAV-SCs. On the other hand,  $W^{AS}$  is the amount of  $W^{REL}$  BW that is assigned by the MCs to the areas not covered by the UAV-SCs. Clearly, it holds that  $W^{AS} \leq W^{REL}$ . By observing in more detail Fig. 10(c), we can note that  $W^{AS} = W^{REL} = 0$  for low values of  $R^{RATE}$ , since no UAV-SC is used. Then, when  $R^{RATE}$  is increased, the UAV-SCs are exploited. This induces a positive  $W^{REL}$ , which is entirely consumed by  $W^{AS}$ . In other words, all the BW released by the areas covered by the UAV-SC is used to enhance the BW of the areas not covered by any UAV-SC. This is valid up to a certain threshold of  $R^{RATE}$  (close to 0.001 [NZD/Mbps]), after which  $W^{AS} < W^{REL}$ , i.e., not all the released BW is assigned to the areas uncovered by UAV-SCs. By further investigating this issue, we verify that this condition occurs when: i) a large amount of areas is covered by UAV-SCs (typically more than 50%), ii) there are sites in which all the corresponding areas are served by UAV-SCs. At last, when the UAV-SCs cover all the areas,  $W^{REL}$  is maximized, while  $W^{AS} = 0$ . However, we point out that, even in this condition, the released BW is not lost, but it is stored in the variables  $\gamma_s^t$ . Therefore, this surplus of BW can be redistributed to other part of the territory covered by the MCs (i.e., the extra BW zones reported in Fig. 1).

Eventually, we consider the paths that are used by the UAV-SCs when moving from the sites to the covered areas. Fig. 11(a) reports the outcome of BBSR for  $R^{RATE} = 0.0012$  [NZD/Mbps]. The colored links mark the paths that are activated. In this case, there are paths in which the recharging site and the served area are pretty close (see e.g., the path between site 4 and area 5). However, there are also paths characterized by a longer distance (see e.g., the path between site 4 and area 10). Moreover, we can observe that most of the areas are not served by any UAV-SC. Fig. 11(b) draws the picture when the weight revenue

<sup>15</sup> We recall that in our scenario we have set a number of UAV-SCs  $|U| = 2 \cdot |A|$ .

$R^{\text{RATE}}$  is increased to 0.01 [NZD/Mbps]. As expected, all the areas are now served by UAV-SCs. Furthermore, most of the paths are characterized by a long distance between the recharging site and the covered area. A natural question is then: why are longer paths preferred compared to shorter ones? To answer this question, we recall the computation of the horizontal speed  $H_l$ , appearing in Eq. (19). According to Eq. (19), when the distance between a site and an area is increased,  $H_l$  is increased. This allows to better exploit the lift force, and consequently to decrease the level flight energy consumption of Eq. (18).<sup>16</sup> As a result, the UAV-SC consumes less energy when the distance between the recharging site and the serving area is increased.

Finally, we refer the reader to Appendix L for a detailed discussion about additional energy constraints, including: i) the charging speed of each UAV-SC, ii) the power ratio between the energy produced by the SPs in each site and the energy demanded by the UAV-SCs, and iii) the number of simultaneous UAV-SC REC actions in each site.

## 8 CONCLUSIONS AND FUTURE WORK

We have focused on the optimization of the energy that is sold to the grid, the energy that is bought from the grid, and the throughput provided to a set of areas in a UAV-aided cellular network. We have modeled the problem by proposing the J-MATE formulation, which is able to adequately take into account all the revenue/cost terms associated to energy and throughput. In addition, we have proposed an efficient heuristic, called BBSR, to solve the problem even for instances composed of hundreds of TSs, which can not be tackled by state-of-the-art optimization tools. Our approaches integrate innovative features, like the redistribution of the MCs BW as a consequence of the UAV-SCs coverage, detailed consumption models for the ground sites and the UAV-SCs, and an MP graph approach to control the UAV-SC missions. Results, obtained over a realistic scenario, demonstrate the superiority of J-MATE and BBSR w.r.t. the competing solutions. In addition, BBSR is able to reduce both the computation time and the memory occupation of five orders of magnitude compared to J-MATE.

We believe that the presented approach can be extended in a number of directions. First, the possibility to exploit multiple UAV-SCs that simultaneously cooperate to serve the same area is an interesting topic. This step could also integrate a more detailed RRM approach, tailored to single users and different services. Second, the impact of introducing other renewable energy sources (e.g., wind turbines, biogas plants) should be considered. Third, the design of smart algorithms based on machine learning approaches to react to unexpected events/failures should be considered, given the increasingly popularity of UAVs and the demand for communications. Fourth, we plan to study the RRM between the UAV-SC and the single users in the covered area. This step should also take into account selected cases where users are in Non Line of Sight (NLOS) conditions w.r.t. the UAV-SC (e.g., those ones inside the buildings). Fifth, the deployment of flexible UAV-based networks, able

16. We remind that a thorough discussion about this aspect is reported in Appendix G.

to track the variation over time of the areas that need to be covered, is another future research agenda.

## ACKNOWLEDGMENTS

This work has received funding from the University of Rome Tor Vergata BRIGHT project (Mission Sustainability Call). We thank Vincent Diao, Sam Madanian, and Jing Ma for their help in performing the measurements for the validation of the UAV-SC energy consumption model.

## REFERENCES

- [1] Y. Zeng, R. Zhang, and T. J. Lim, "Wireless communications with unmanned aerial vehicles: opportunities and challenges," *IEEE Communications Magazine*, vol. 54, no. 5, pp. 36–42, 2016.
- [2] M. Mozaffari, W. Saad, M. Bennis, and M. Debbah, "Drone small cells in the clouds: Design, deployment and performance analysis," in *2015 IEEE Global Communications Conference (GLOBECOM)*, pp. 1–6, San Diego, CA, December 2015.
- [3] R. I. Bor-Yaliniz, A. El-Keyi, and H. Yanikomeroglu, "Efficient 3-D placement of an aerial base station in next generation cellular networks," in *2016 IEEE International Conference on Communications (ICC)*, pp. 1–5, Kuala Lumpur, Malaysia, May 2016.
- [4] A. Fotouhi, H. Qiang, M. Ding, M. Hassan, L. G. Giordano, A. Garcia-Rodriguez, and J. Yuan, "Survey on uav cellular communications: Practical aspects, standardization advancements, regulation, and security challenges," *IEEE Communications Surveys Tutorials*, vol. 21, pp. 3417–3442, Fourthquarter 2019.
- [5] M. Mozaffari, W. Saad, M. Bennis, Y. Nam, and M. Debbah, "A tutorial on uavs for wireless networks: Applications, challenges, and open problems," *IEEE Communications Surveys Tutorials*, vol. 21, pp. 2334–2360, thirdquarter 2019.
- [6] N. Cheng, W. Xu, W. Shi, Y. Zhou, N. Lu, H. Zhou, and X. Shen, "Air-ground integrated mobile edge networks: Architecture, challenges, and opportunities," *IEEE Communications Magazine*, vol. 56, no. 8, pp. 26–32, 2018.
- [7] V. Sharma, M. Bennis, and R. Kumar, "UAV-assisted heterogeneous networks for capacity enhancement," *IEEE Communications Letters*, vol. 20, no. 6, pp. 1207–1210, 2016.
- [8] L. Chiaraviglio, N. Blefari-Melazzi, W. Liu, J. A. Gutierrez, J. van de Beek, R. Birke, L. Chen, F. Idzikowski, D. Kilper, P. Monti, A. Bagula, and J. Wu, "Bringing 5G into Rural and Low-Income Areas: Is It Feasible?," *IEEE Communications Standards Magazine*, vol. 1, no. 3, pp. 50–57, 2017.
- [9] S. A. R. Naqvi, S. A. Hassan, H. Pervaiz, and Q. Ni, "Drone-aided communication as a key enabler for 5G and resilient public safety networks," *IEEE Communications Magazine*, vol. 56, no. 1, pp. 36–42, 2018.
- [10] S. Sekander, H. Tabassum, and E. Hossain, "Multi-tier drone architecture for 5G/B5G cellular networks: Challenges, trends, and prospects," *IEEE Communications Magazine*, vol. 56, no. 3, pp. 96–103, 2018.
- [11] Ø. Magnussen, G. Hovland, and M. Ottestad, "Multicopter UAV design optimization," in *2014 IEEE/ASME 10th International Conference on Mechatronic and Embedded Systems and Applications (MESA)*, pp. 1–6, Senigallia, Italy, September 2014.
- [12] L. Amorosi, L. Chiaraviglio, F. D'Andreagiovanni, and N. Blefari-Melazzi, "Energy-efficient mission planning of UAVs for 5G coverage in rural zones," in *IEEE International Conference on Environmental Engineering (EE)*, pp. 1–9, Milay, Italy, March 2018.
- [13] L. Chiaraviglio, F. D'Andreagiovanni, R. Choo, F. Cuomo, and S. Colonnese, "Joint Optimization of Area Throughput and Grid-Connected Microgeneration in UAV-Based Mobile Networks," *IEEE Access*, vol. 7, pp. 69545–69558, 2019.
- [14] M. Mozaffari, W. Saad, M. Bennis, and M. Debbah, "Efficient deployment of multiple unmanned aerial vehicles for optimal wireless coverage," *IEEE Communications Letters*, vol. 20, no. 8, pp. 1647–1650, 2016.
- [15] H. N. Qureshi and A. Imran, "On the Tradeoffs Between Coverage Radius, Altitude, and Beamwidth for Practical UAV Deployments," *IEEE Transactions on Aerospace and Electronic Systems*, vol. 55, pp. 2805–2821, Dec 2019.

- [16] S. Mignardi and R. Verdone, "On the performance improvement of a cellular network supported by an unmanned aerial base station," in *2017 29th International Teletraffic Congress (ITC 29)*, vol. 2, pp. 7–12, Genoa, Italy, September 2017.
- [17] S. Jeong, O. Simeone, and J. Kang, "Mobile edge computing via a UAV-mounted cloudlet: Optimization of bit allocation and path planning," *IEEE Transactions on Vehicular Technology*, vol. 67, no. 3, pp. 2049–2063, 2018.
- [18] R. Verdone and S. Mignardi, "Joint Aerial-Terrestrial Resource Management in UAV-Aided Mobile Radio Networks," *IEEE Network*, vol. 32, no. 5, pp. 70–75, 2018.
- [19] Q. Wu, Y. Zeng, and R. Zhang, "Joint trajectory and communication design for multi-UAV enabled wireless networks," *IEEE Transactions on Wireless Communications*, vol. 17, no. 3, pp. 2109–2121, 2018.
- [20] K. Zhu, X. Xu, and S. Han, "Energy-Efficient UAV Trajectory Planning for Data Collection and Computation in mMTC Networks," in *2018 IEEE Globecom Workshops (GC Wkshps)*, pp. 1–6, Abu Dhabi, UAE, December 2018.
- [21] R. Li, Z. Wei, L. Yang, D. W. Kwan Ng, N. Yang, J. Yuan, and J. An, "Joint Trajectory and Resource Allocation Design for UAV Communication Systems," in *2018 IEEE Globecom Workshops (GC Wkshps)*, pp. 1–6, Abu Dhabi, UAE, December 2018.
- [22] A. Mardani, M. Chiaberge, and P. Giaccone, "Communication-Aware UAV Path Planning," in *2018 6th IEEE International Conference on Wireless for Space and Extreme Environments (WiSEE)*, Huntsville, AL, December 2018.
- [23] Y. Zeng, J. Lyu, and R. Zhang, "Cellular-Connected UAV: Potential, Challenges, and Promising Technologies," *IEEE Wireless Communications*, vol. 26, no. 1, pp. 120–127, 2019.
- [24] A. Trotta, M. D. Felice, F. Montori, K. R. Chowdhury, and L. Bononi, "Joint Coverage, Connectivity, and Charging Strategies for Distributed UAV Networks," *IEEE Trans. on Robotics*, vol. 34, no. 4, pp. 883–900, 2018.
- [25] Q. Wu, L. Liu, and R. Zhang, "Fundamental Trade-offs in Communication and Trajectory Design for UAV-Enabled Wireless Network," *IEEE Wireless Communications*, vol. 26, no. 1, pp. 36–44, 2019.
- [26] M. Hua, Y. Wang, C. Li, Y. Huang, and L. Yang, "Energy-Efficient Optimization for UAV-Aided Cellular Offloading," *IEEE Wireless Communications Letters*, vol. 8, no. 3, pp. 769–772, 2019.
- [27] Y. Sun, D. Xu, D. W. K. Ng, L. Dai, and R. Schober, "Optimal 3D-Trajectory Design and Resource Allocation for Solar-Powered UAV Communication Systems," *IEEE Transactions on Communications*, vol. 67, no. 6, pp. 4281–4298, 2019.
- [28] "3GPP 36.881 Study on latency reduction techniques for LTE." <https://portal.3gpp.org/desktopmodules/Specifications/SpecificationDetails.aspx?specificationId=2901>, 2015. Last Accessed: 2nd Jan. 2020.
- [29] Y. Zeng, Q. Wu, and R. Zhang, "Accessing From the Sky: A Tutorial on UAV Communications for 5G and Beyond," *Proceedings of the IEEE*, vol. 107, pp. 2327–2375, Dec 2019.
- [30] X. Cai, A. Gonzalez-Plaza, D. Alonso, L. Zhang, C. B. Rodríguez, A. P. Yuste, and X. Yin, "Low altitude UAV propagation channel modelling," in *2017 11th European Conference on Antennas and Propagation (EUCAP)*, pp. 1443–1447, Paris, France, March 2017.
- [31] M. R. Garey and D. S. Johnson, "Computers and Intractability: A Guide to the Theory of NP-Completeness," 1979.
- [32] "CellMapper." <https://www.cellmapper.net>. Last Accessed: 26th July 2019.
- [33] "Small Cell Networks and the Evolution of 5G." <https://www.qorvo.com/design-hub/blog/small-cell-networks-and-the-evolution-of-5>. Last Accessed: 7th Aug. 2019.
- [34] S. Colonnese, F. Cuomo, L. Chiaravaggio, V. Salvatore, T. Melodia, and I. Rubin, "CLEVER: A Cooperative and Cross-Layer Approach to Video Streaming in HetNets," *IEEE Transactions on Mobile Computing*, vol. 17, no. 7, pp. 1497–1510, 2018.
- [35] J. Seddon and S. Newman, *Basic helicopter aerodynamics*. American Institute of Aeronautics and Astronautics, 2001.
- [36] B. H. Jung, H. Leem, and D. K. Sung, "Modeling of power consumption for macro-, micro-, and RRH-based base station architectures," in *2014 IEEE 79th Vehicular Technology Conference (VTC Spring)*, pp. 1–5, Seoul, Korea, May 2014.
- [37] B. Marion and M. Anderberg, "PVWATTS - an online performance calculator for grid-connected PV systems," in *Proc. of the Solar Conference*, pp. 119–124, Madison, WI, June 2000.
- [38] "Domestic Generation." <https://www.trustpower.co.nz/our-assets-and-capability/power-generation/domestic-generation>. Last Accessed: 23rd July 2019.
- [39] "NZ Electricity Authority Wholesale information and trading system (WITS)." <https://www.ea.govt.nz/operations/wholesale/spot-pricing/wits/>. Last Accessed: 21st Dec. 2018.
- [40] C. Ide, R. Falkenberg, D. Kaulbars, and C. Wietfeld, "Empirical analysis of the impact of LTE downlink channel indicators on the uplink connectivity," in *2016 IEEE 83rd Vehicular Technology Conference (VTC Spring)*, pp. 1–5, Nanjing, China, May 2016.
- [41] R. Amorim, H. Nguyen, P. Mogensen, I. Z. Kovács, J. Wigard, and T. B. Sørensen, "Radio channel modeling for UAV communication over cellular networks," *IEEE Wireless Communications Letters*, vol. 6, no. 4, pp. 514–517, 2017.
- [42] D. W. Matolak and R. Sun, "Air-ground channel characterization for unmanned aircraft systems-Part III: The suburban and near-urban environments," *IEEE Transactions on Vehicular Technology*, vol. 66, no. 8, pp. 6607–6618, 2017.
- [43] "US-1 Specifications." <https://impossible.aero/us-1/>. Last Accessed: 3rd Jan. 2020.



**Luca Chiaravaggio** (M'09-SM'16) is Associate Professor at the University of Rome Tor Vergata (Italy). He holds a Ph.D. in Telecommunication and Electronics Engineering, obtained from Politecnico di Torino (Italy). Luca has co-authored 130+ papers published in international journals, books and conferences. He participates in the TPC of IEEE INFOCOM, IEEE GLOBECOM, IEEE ICC, IEEE VTC and IEEE GlobalSIP. He has received the Best Paper Award in different conferences, including IEEE VTC and ICIN. His

current research topics cover 5G networks, cloud computing, optimization applied to telecommunication networks, new architectures to reduce the digital divide in rural and low-income areas and electromagnetic fields.



**Fabio D'Andreagiovanni** has been a First Class Research Scientist at the French National Center for Scientific Research (CNRS) since October 2016. Until September 2016, he was Head of Research Group at the Department of Mathematical Optimization of Zuse Institute Berlin and Lecturer at the Department of Mathematics and Computer Science of Free University Berlin and at the Faculty of Mechanical Engineering of Technical University Berlin. He received his M.Sc. in Industrial Engineering (2006) and Ph.D.

in Operations Research (2010) from University of Rome Sapienza and he was Research Scholar of the Department of Industrial Engineering and Operations Research at Columbia University in the City of New York (2008-2009). His research has been focused on the theory and applications of Robust Optimization and Mixed Integer Programming and has received many awards for his work, such as the Accenture M.Sc. Prize 2006, the INFORMS Telecom Ph.D. Award 2010 and Best Paper Award 2014, the RNDM Best Paper Award 2017, and the ICIN Best Paper Award 2018. He has worked as consultant for various major European telecommunications and electric utility companies.



**William Liu** received his Master (with distinction) and PhD in Electrical and Computer Engineering at the University of Canterbury, Christchurch, New Zealand, in 2005 and 2010 respectively. He is currently a Senior Lecturer at the Department of Information Technology and Software Engineering, School of Engineering, Computer and Mathematical Sciences, Auckland University of Technology. In general, his research interests are in the design and performance evaluation on packet-oriented networks.

He is working especially in the areas of network survivability, sustainability, and trustworthy computing.



**Kim-Kwang Raymond Choo** (SM'15) received the Ph.D. in Information Security in 2006 from Queensland University of Technology, Australia. He currently holds the Cloud Technology Endowed Professorship at The University of Texas at San Antonio (UTSA), and has a courtesy appointment at the University of South Australia. In 2016, he was named the Cybersecurity Educator of the Year - APAC (Cybersecurity Excellence Awards are produced in cooperation with the Information Security Community on LinkedIn), and

in 2015 he and his team won the Digital Forensics Research Challenge organized by Germany's University of Erlangen-Nuremberg. He is the recipient of the 2018 UTSA College of Business Col. Jean Piccione and Lt. Col. Philip Piccione Endowed Research Award for Tenured Faculty, ESORICS 2015 Best Paper Award, 2014 Highly Commended Award by the Australia New Zealand Policing Advisory Agency, Fulbright Scholarship in 2009, 2008 Australia Day Achievement Medallion, and British Computer Society's Wilkes Award in 2008. He is also a Fellow of the Australian Computer Society, and he is an IEEE Senior Member.



**Jairo A. Gutierrez** is Professor of Information Technology and Deputy Head of the School of Engineering, Computer and Mathematical Sciences at Auckland University of Technology in New Zealand. He was the Editor-in-Chief of the International Journal of Business Data Communications and Networking (2004-2008) and received a Systems and Computing Engineering degree from Universidad de Los Andes in Colombia, a Masters degree in Computer Science from Texas A&M University, and a Ph.D. in

Information Systems from the University of Auckland. His current research is on network management systems, networking security, viable business models for IT-enabled enterprises, next-generation networks and cloud computing systems.



**Mohamed Slim Alouini** (S94-M98-SM03-F09) was born in Tunis, Tunisia. He received the Ph.D. degree in Electrical Engineering from the California Institute of Technology (Caltech), Pasadena, CA, USA, in 1998. He served as a faculty member in the University of Minnesota, Minneapolis, MN, USA, then in the Texas A&M University at Qatar, Education City, Doha, Qatar before joining King Abdullah University of Science and Technology (KAUST), Thuwal, Makkah Province, Saudi Arabia as a Professor of Electrical Engineering in 2009. His current research interests include the modeling, design, and performance analysis of wireless communication systems.



**Nicola Belfari-Melazzi** is currently a Full Professor of telecommunications with the University of Rome "Tor Vergata", Italy. He is currently the Director of CNIT, a consortium of 37 Italian Universities. He has participated in over 30 international projects, and has been the principal investigator of several EU funded projects. He has been an Evaluator for many research proposals and a Reviewer for numerous EU projects. He is the author/coauthor of about 200 articles, in international journals and conference proceedings. His research interests include the performance evaluation, design and control of broadband integrated networks, wireless LANs, satellite networks, and of the Internet. He has also worked on multimedia traffic modeling, mobile and personal communications, quality of service in the Internet, ubiquitous computing, reconfigurable systems and networks, service personalization, autonomic computing, SDN/NFV, and ICT solutions for intelligent transport systems